International Journal of Thermophysics, Vol. 14, No. 4, 1993

Transport Properties of 1,1,1,2-Tetrafluoroethane (R134a)[1]

R. Krauss,[2] J. Luettmer-Strathmann,[3] J. V. Sengers,[3,4] and K. Stephan[2]

Received March 23, 1993

New equations for the thermal conductivity and the viscosity of R134a that are valid in a wide range of pressures and temperatures are presented. They were obtained through a theoretically based, critical evaluation of the available experimental data, which showed considerable inconsistencies between data sets, in particular in the vapor phase. In the critical region the observed enhancement in the thermal conductivity is well represented by a crossover model for the transport properties of fluids. Since thermodynamic properties enter into the calculation of the critical enhancement of the transport properties, a new fundamental equation for the critical region was developed also.

KEY WORDS: 1,1,1,2-tetrafluoroethane; correlation; critical region; equation of state; HFC-134a; R134a; thermal conductivity; transport properties; viscosity.

1. INTRODUCTION

Since R134a (1,1,1,2-tetrafluoroethane) is considered to be an environmentally acceptable alternative to the now commonly used, but ozone depleting refrigerant R12 (dichlorodifluoromethane), there has recently been a great interest in its thermophysical properties, including its transport properties. Unfortunately the amount of experimental data available is still small and different data sets are often inconsistent. An evaluation and correlation of the transport properties of R134a was published recently by some of the

[1] Paper dedicated to Professor Joseph Kestin.

[2] Institut für Technische Thermodynamik und Thermische Verfahrenstechnik, Universität Stuttgart, Pfaffenwaldring 9, D 7000 Stuttgart 80, Germany.

[3] Institute for Physical Science and Technology, University of Maryland, College Park, Maryland 20742, U.S.A.

[4] Thermophysics Division, National Institute of Standards and Technology, Gaithersburg, Maryland 20899, U.S.A.

0195-928X/93/0700-0951$07.00/0

authors [1], but without taking any critical enhancement of the transport coefficients into account. Since, for the thermal conductivity, the effects of critical fluctuations extend over a wide range of temperatures and densities [2, 3], a considerable amount of data had to be excluded from the analysis. The critical enhancement of the thermal conductivity of R134a was considered by Laesecke et al. [4] in the evaluation of their own experimental thermal-conductivity data, but they used a classical equation of state throughout their analysis. In the meantime new series of measurements of the transport properties of R134a have become available, so that some data gaps could be filled. It is the purpose of this work to investigate in detail the available information for the thermal conductivity and the viscosity of R134a including data in the critical region.

2. METHODOLOGY

The correlation of the viscosity and thermal conductivity is based on the residual concept. The viscosity $\eta(\rho, T)$ and the thermal conductivity $\lambda(\rho, T)$ of a pure fluid at density ρ and temperature T may be considered as composed of three different contributions [5, 6]:

(i) a dilute-gas term $\eta_0(T)$ and $\lambda_0(T)$, respectively, that depends on temperature only,

(ii) an excess or residual term $\Delta_R\eta(\rho, T)$ and $\Delta_R\lambda(\rho, T)$, respectively, that accounts for the density dependence, and

(iii) a contribution $\Delta_c\eta(\rho, T)$ and $\Delta_c\lambda(\rho, T)$, respectively, that represents the critical enhancement in a region extending around the vapor–liquid critical point [2].

Some theoretical guidance about the temperature dependence of the transport properties $\eta_0(T)$ and $\lambda_0(T)$ of a dilute gas can be obtained from the kinetic theory of gases [7]. A theory for the enhancement $\Delta_c\eta(\rho, T)$ and $\Delta_c\lambda(\rho, T)$ due to critical fluctuations has been proposed by Olchowy and Sengers [8, 9]. For the excess contributions $\Delta_R\eta(\rho, T)$ and $\Delta_R\lambda(\rho, T)$ of a real gas, no reliable theoretical expressions are available, but it has been found empirically that they depend at moderate pressures only weakly on the temperature. As was found for other fluids [5, 8], for R134a the temperature dependence of the excess terms may be neglected in the pressure and temperature range of interest, because the resulting errors are smaller than the experimental uncertainties. We thus represent the transport properties of R134a by equations of the form

$$\eta(\rho, T) = \eta_0(T) + \Delta_R\eta(\rho) + \Delta_c\eta(\rho, T) \tag{1}$$

and

$$\lambda(\rho, T) = \lambda_0(T) + \Delta_R \lambda(\rho) + \Delta_c \lambda(\rho, T) \tag{2}$$

The dilute-gas and excess terms do not contain any contributions from long-range critical fluctuations and they together represent what we refer to as the background transport properties $\bar{\eta}$ and $\bar{\lambda}$ [2]

$$\bar{\eta} = \eta_0(T) + \Delta_R \eta(\rho) \tag{3}$$

$$\bar{\lambda} = \lambda_0(T) + \Delta_R \lambda(\rho) \tag{4}$$

It has been established that the critical viscosity enhancement $\Delta_c \eta(\rho, T)$ is small and becomes relevant only at temperatures and densities extremely close to the critical point [8]. For R134a no experimental viscosity data are available so close to the critical point and the background viscosity can be directly identified with the actual available experimental viscosity η_{expt}:

$$\bar{\eta}(\rho, T) = \eta_{expt}(\rho, T) \tag{5}$$

However, the critical thermal-conductivity enhancement $\Delta_c \lambda(\rho, T)$ is significant in a large range of temperatures and densities and $\bar{\lambda}$ is in practice deduced from the experimental thermal conductivity λ_{expt} as

$$\bar{\lambda}(\rho, T) = \lambda_{expt}(\rho, T) - \Delta_c \lambda(\rho, T) \tag{6}$$

The theory of Olchowy and Sengers yields expressions that relate $\Delta_c \eta$ and $\Delta_c \lambda$ to various thermodynamic properties to be deduced from a comprehensive equation of state and to the background transport properties $\bar{\eta}$ and $\bar{\lambda}$, while containing one system-dependent parameter q_D that determines the maximum wave number of the collective critical fluctuations. Starting from an initial theoretical estimate for $\Delta_c \lambda(\rho, T)$, the contributions $\bar{\lambda}$ and $\Delta_c \lambda$ are then determined by an iterative process until a satisfactory representation of the experimental data is obtained [4, 5, 8].

3. DILUTE-GAS FUNCTIONS

The contributions of the transport properties in the zero-density limit, $\eta_0(T)$ and $\lambda_0(T)$, may be treated independently from the excess terms and the critical-enhancement terms. Therefore one usually starts the correlation procedure with the determination of the dilute-gas functions. Since zero-density data of either property are lacking, we used data measured at atmospheric pressure or below. Due to the scattering of the data sets, this is justified because the resulting error lies within the precision of the measurements.

3.1. Viscosity

Experimental data in the vapor phase at atmospheric pressure were obtained from the work of Nabizadeh and Mayinger [10], Takahashi et al. [11], and Dowdell and Matthews [12]. Since the data of Takahashi et al. [11] have been presented only in the form of graphs and equations, we used their correlation to calculate quasi-experimental viscosity data at the corresponding temperatures. We have also extrapolated two isotherms of Ruvinskii et al. [13] to zero density. Both Nabizadeh and Mayinger [10] and Takahashi et al. [11] used an oscillating-disk apparatus, whereas the measurements of Dowdell and Matthews [12] and of Ruvinskii et al. [13] were obtained with a capillary viscometer. In addition, Oliveira and Wakeham have obtained viscosity data for the saturated vapor with a vibrating-wire apparatus [14]. Our correlation is based on the measurements of Nabizadeh and Mayinger [10], of Takahashi et al. [11], and of Dowdell and Matthews [12].

The dilute-gas viscosity η_0 is represented by an expression derived from the kinetic theory of gases,

$$\eta_0 = \frac{5}{16}\sqrt{\frac{MkT}{\pi N_A}}\frac{10^{24}}{\sigma^2\Omega_\eta(T^*)} = \frac{0.2696566\sqrt{T}}{\sigma^2\Omega_\eta(T^*)} \tag{7}$$

where $M = 0.10203\ \mathrm{kg \cdot mol^{-1}}$ is the molecular weight, k is Boltzmann's constant in $\mathrm{J \cdot K^{-1}}$, and N_A is Avogadro's number in $\mathrm{mol^{-1}}$. The viscosity η_0 has units $\mu\mathrm{Pa \cdot s}$, the temperature T is given in K, and the length scaling factor σ in nm. The dimensionless temperature T^* is defined as

$$T^* = kT/\varepsilon \tag{8}$$

where the energy and length scaling factors ε/k and σ, respectively, were estimated by means of a least-squares fit:

$$\varepsilon/k = 279.86\ \mathrm{K}, \qquad \sigma = 0.50768\ \mathrm{nm} \tag{9}$$

For the collision integral Ω_η as a function of T^*, we adopted a formula presented by Bich et al. [15],

$$\ln \Omega_\eta(T^*) = \sum_{i=0}^{4} a_i (\ln T^*)^i \tag{10}$$

with coefficients a_i

$$\begin{aligned} a_0 &= 0.4425728, \qquad a_1 = -0.5138403, \qquad a_2 = 0.1547566 \\ a_3 &= -0.02821844, \qquad a_4 = 0.001578286 \end{aligned} \tag{11}$$

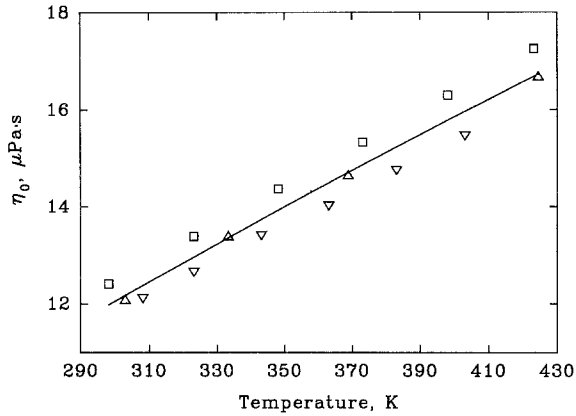

Fig. 1. The viscosity of R134a in the dilute-gas limit. The solid line represents the values as calculated from Eq. (7); the data points are those reported by Nabizadeh and Mayinger [10], △; Takahashi et al. [11], □; and Dowdell and Matthews [12], ▽.

The viscosity η_0 in the dilute-gas limit is shown in Fig. 1 as a function of temperature, while the deviations of the experimental data from the correlation are shown in Fig. 2. Although the results of Takahashi et al. [11] are available only in functional form, we have represented them in Fig. 1 by symbols to show the individual data points used for the present

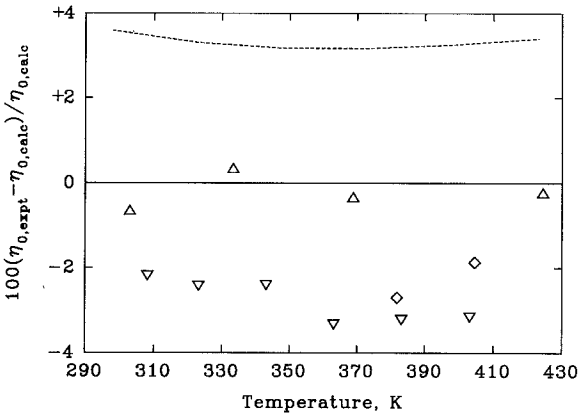

Fig. 2. Relative deviations of the experimental viscosity data of Nabizadeh and Mayinger [10] △, Dowdell and Matthews [12] ▽, and Ruvinskii et al. [13] ◇ from values calculated with the dilute-gas function $\eta_0(T)$, Eq. (7). The dashed line represents the correlation of Takahashi et al. [11].

correlation. It is obvious that there exist systematic deviations among the data sets of Nabizadeh and Mayinger [10], Takahashi et al. [11], and Dowdell and Matthews [12]. Equation (7) represents the available experimental information for η_0 within $\pm 4\%$ at temperatures from 290 to 430 K. Because of the theoretical basis of Eq. (7), we expect that it can be extrapolated outside this temperature range with only a modest loss of accuracy.

3.2. Thermal Conductivity

Data at atmospheric pressure or below have been reported by Ross et al. [16], Ruvinskii et al. [13], Laesecke et al. [4], Gross et al. [17], and Taxis and Stephan [18]. These data seem to be the most reliable ones in this region and therefore they were used to determine the dilute-gas function λ_0. Additional data have been reported by Shankland et al. [19], Tanaka et al. [20], and Yamamoto et al. [21]. With the exception of Ruvinskii et al. [13], who used a steady state hot-wire apparatus, and Tanaka et al. [20], who used a coaxial-cylinder apparatus, the measurements have been obtained with a transient hot-wire apparatus. As both Laesecke et al. [4] and Gross et al. [17] have established a dilute-gas function based on their own measurements, we used these correlations to calculate quasi-experimental thermal-conductivity data at the corresponding temperatures.

Since a theoretical treatment of the dilute-gas function is complicated by contributions from internal degrees of freedom [5], we represent λ_0 by an empirical equation of the form

$$\lambda_0 = -16.5744 + 0.124286T - 0.761796 \times 10^{-4} T^2 \tag{12}$$

with λ_0 in $\mathrm{mW \cdot m^{-1} \cdot K^{-1}}$ and the temperature T in K. The thermal conductivity λ_0 in the dilute-gas limit is shown in Fig. 3 as a function of temperature. The data of Laesecke et al. [4] and Gross et al. [17] are represented by symbols, although they are available in functional form, to demonstrate the individual data points that were used for the present correlation. Equation (12) is valid at temperatures from 240 to 410 K, but we had to use it for temperatures up to 425 K in the remainder of this work. Figure 4 shows the deviations of all experimental data relative to the dilute-gas function λ_0 as given by Eq. (12). The data of Shankland et al. [19], Yamamoto et al. [21], and Tanaka et al. [20] show appreciable systematic deviations.

The correlation has an uncertainty of 1.5% except at the lower and upper temperature ranges, where the uncertainty rises to 3 and 5%,

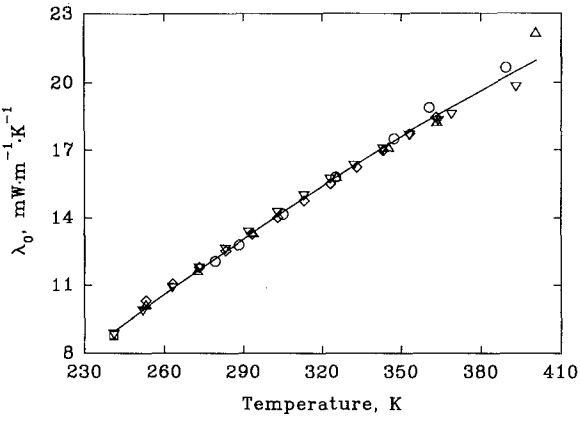

Fig. 3. The thermal conductivity of R134a in the dilute-gas limit. The solid line represents the values as calculated from Eq. (12); the data points are those reported by Laesecke et al. [4], ▽; Ruvinskii et al. [13], △; Ross et al. [16], □; Gross et al. [17], ◇; and Taxis and Stephan [18], ○.

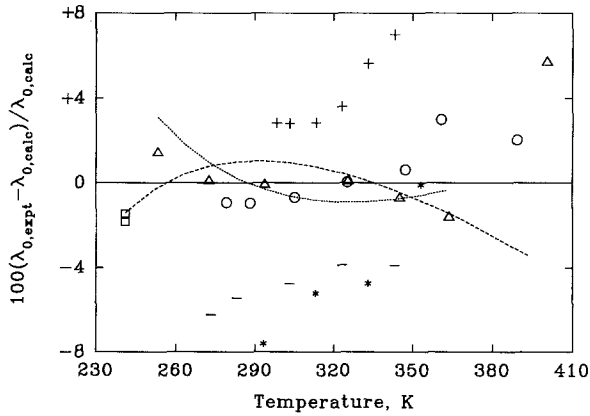

Fig. 4. Relative deviations of the experimental thermal-conductivity data of Ruvinskii et al. [13] △, Ross et al. [16] □, Taxis and Stephan [18] ○, Shankland et al. [19] +, Tanaka et al. [20] *, and Yamamoto et al. [21] — from the values calculated with the dilute-gas function $\lambda_0(T)$, Eq. (12) for the thermal conductivity. The dashed line represents the correlation of Laesecke et al. [4]; the dotted line, the correlation of Gross et al. [17].

respectively. It is obvious that there exist discrepancies especially at higher temperatures that are well beyond the precision of the individual measurements.

4. EXCESS FUNCTIONS

In order to calculate the residual part $\Delta_R\eta(\rho)$ of the viscosity or $\Delta_R\lambda(\rho)$ of the thermal conductivity, the dilute-gas term and the critical-enhancement term must be subtracted from the total quantity. The residual or excess quantities thus found mainly depend on density, and only weakly on temperature. As for other substances [5, 6], the temperature dependence may be neglected in the case of the excess viscosity and the excess thermal conductivity of R134a, because the resulting error lies within the experimental accuracy.

Whenever possible, we used dilute-gas data or data at atmospheric pressure reported by the authors themselves. The critical enhancement of the thermal conductivity will be treated in Section 5.2. As already mentioned, a critical enhancement has not been observed in the viscosity data available for R134a.

In order to avoid exorbitant deviations that are due to the extremely small excess values at low densities, the deviations in the following subsections were calculated after adding the corresponding dilute-gas contribution to each excess value. That is, the deviations refer to the background transport properties $\bar{\eta}$ and $\bar{\lambda}$ rather than to $\Delta_R\eta(\rho)$ and $\Delta_R\lambda(\rho)$.

4.1. VISCOSITY

The correlation of the residual viscosity or excess viscosity, respectively, is based on the data of Takahashi et al. [11] in the vapor phase and the measurements of Oliveira and Wakeham [22] and Okubo et al. [23] in the liquid phase. Oliveira and Wakeham used a vibrating-wire apparatus, whereas Okubo et al. used a capillary viscometer. The reduced viscosity can be represented as a function of the reduced density by a third-order polynomial with a hyperbolic term that accounts for the steep increase of the viscosity at high densities [6]. Hence

$$\frac{\Delta_R\eta}{H_c} = \sum_{i=1}^{3} e_i \left(\frac{\rho}{\rho_c}\right)^i + \frac{e_4}{\rho/\rho_c - e_5} + \frac{e_4}{e_5} \tag{13}$$

where $\rho_c = 515.25\ \mathrm{kg \cdot m^{-3}}$ is the critical density [24] and H_c is a so-called pseudo-critical viscosity [6] defined as

$$H_c = \frac{M^{1/2} P_c^{2/3}}{R^{1/6} N_A^{1/3} T_c^{1/6}} = 25.21\ \mu\mathrm{Pa \cdot s} \tag{14}$$

In Eq. (14) R is the universal molar gas constant, $P_c = 4.065$ MPa the critical pressure, and $T_c = 374.274$ K the critical temperature. The coefficients in Eq. (13) are

$$\begin{aligned} e_1 &= -1.89758, \quad e_2 = 0.256449, \quad e_3 = -0.301641 \\ e_4 &= -23.1648, \quad e_5 = 3.44752 \end{aligned} \tag{15}$$

Equation (13) is valid in the temperature range from 290 K to 430 K and up to $1400\ \mathrm{kg \cdot m^{-3}}$.

Figure 5 shows the selected excess data together with the correlation function that is represented by a solid line. The corresponding deviation plot, shown in Fig. 6, reveals an uncertainty of approximately 2% in the vapor phase and 3% in the liquid region. In the vapor phase a temperature dependence of the excess values implied by the data of Takahashi et al. [11] is recognizable, but it lies within the overall uncertainty of the correlation of the viscosity.

Figure 7 shows deviations of the experimental data sets that were not used for the correlation. Although the data of Nabizadeh and Mayinger

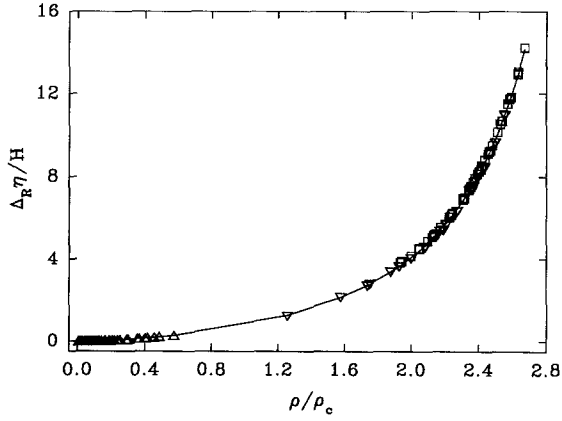

Fig. 5. The excess function for the viscosity of R134a. The solid line represents values calculated from Eq. (13); the data points are those reported by Takahashi et al. [11], △; Oliveira and Wakeham [22], □; and Okubo et al. [23], ▽.

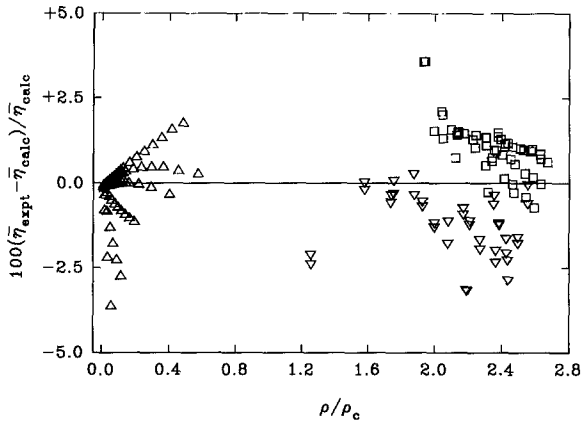

Fig. 6. Relative deviations of the experimental data of Takahashi et al. [11] △, Oliveira and Wakeham [22] □, and Okubo et al. [23] ▽ from values calculated with Eqs. (7) and (13) for the background viscosity $\bar{\eta}=\eta_0+\Delta_R\eta$.

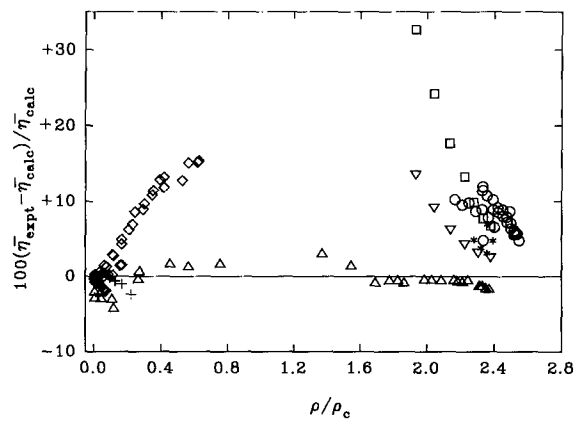

Fig. 7. Relative deviations of the experimental data of Nabizadeh and Mayinger [10] ◇, Ruvinskii et al. [13] △, Wakeham and Oliveira [14] +, Shankland et al. [19] □, Kumagai and Takahashi [25] ▽, Diller et al. [26] ○, and Ripple and Matar [27] * from values calculated with Eqs. (7) and (13) for the background viscosity $\bar{\eta}=\eta_0+\Delta_R\eta$.

[10] in the dilute-gas region seem to be reliable, the density dependence of their data turned out to be too strong. This is also the case for the saturated-liquid data reported by Shankland et al. [19] and by Kumagai and Takahashi [25] and for the data of Diller et al. [26] in the liquid phase. The saturated-liquid data reported by Ripple and Matar [27] is about 5% higher than the correlation, whereas the accuracy of their apparatus is approximately 3%. The data of Ruvinskii et al. [13] and the data of Oliveira and Wakeham [14] near saturation agree quite well with the correlation.

References reporting experimental data are compiled in Table I together with the name of the first author, the physical state and the total pressure and temperature range of the reported experimental data, the number of points used for comparison, the experimental method, the absolute mean error, and the maximum error of each data set relative to the present correlation. Please note that we have compared only those experimental data points that are within the range of validity of the correlation and that are shown in the deviation plots. The temperature and pressure ranges listed in Table I are the ranges which experiments were carried out by the individual authors and are therefore sometimes wider than the range of comparison.

In a viscosity–density and a viscosity–pressure diagram, respectively, the slopes of the isotherms in the vapor phase become negative at temperatures that are lower than a specific inversion temperature. The negative

Table I. Comparison of Experimental Viscosity Data with the Correlation[a]

Ref. No.	Author	Physical state	P_{min} (MPa)	P_{max} (MPa)	T_{min} (K)	T_{max} (K)	Points compared	Method	Mean error (%)	Maximum error (%)
10	Nabizadeh	v	0.1	6.4	303	424	41	od	4.7	15.
11	Takahashi	v	0.1	5.5	298	423	71	od	3.0	4.4
12	Dowdell	v	0.1	0.1	308	403	6	cv	2.9	−3.4
13	Ruvinskii	v, l	0	6.4	258	405	29	cv	1.4	−4.0
14	Oliveira	sv	0.1	2.1	243	343	6	vw	0.8	−2.4
19	Shankland	sl	0.1	2.1	251	343	7	cv	16.	32.
22	Oliveira	l, sl	0.1	51	238	343	49	vw	1.1	3.6
23	Okubo	l	1.6	30.2	213	423	39	cv	1.3	−3.2
25	Kumagai	sl	0.3	2.1	273	343	6	cv	6.5	14.
26	Diller	l, sl	<0.1	33.7	175	320	27	tc	8.1	12.
27	Ripple	sl	0.1	0.8	250	306	5	cv	4.7	7.0

[a] v, vapor; l, liquid; sl, saturated liquid; sv, saturated vapor; cv, capillary viscometer; od, oscillating disk; tc, torsional crystal; vw, vibrating wire.

slope increases with decreasing temperature. Then the isotherms of the excess viscosity no longer coincide and the residual concept used for the present correlation procedure is no longer applicable because the temperature dependence becomes significant. For R134a the inversion temperature below which the slopes become negative seems to be between 290 and 300 K [10, 11]. Hence below that temperature in the vapor phase the correlation function should not be used.

4.2. Thermal Conductivity

The excess function of the thermal conductivity is based on the measurements of Taxis and Stephan [18], Ross et al. [16], and Kruppa and Straub [28] in the vapor phase and of Schmitt [29], Ross et al. [16], Yata et al. [30], Ueno et al. [31], Oliveira et al. [32], Leipertz and Kraft [33], and Kruppa and Straub [28] in the liquid phase. Kruppa and Straub [28] and Leipertz and Kraft [33] actually measured the thermal diffusivity D_T by means of dynamic light scattering. We calculated the corresponding thermal conductivity λ using the relation $\lambda = \rho c_P D_T$, where c_P is the isobaric specific heat calculated from a fundamental equation to be presented in Section 5.1. In order to fill the data gaps in the extended region around the critical density, we used selected data of Kruppa and Straub [28] at about 370 and 393 K. For details on the calculations in the critical region see Section 5.2.

The excess data can be represented by a fourth-order polynomial of the form

$$\frac{\Lambda_R \lambda_t}{\Lambda_c} = \sum_{i=1}^{4} l_i \left(\frac{\rho}{\rho_c}\right)^i \tag{16}$$

where $\rho_c = 515.25\ \mathrm{kg \cdot m^{-3}}$ is the critical density as in Eq. (13), while Λ_c is a so-called pseudo-critical thermal conductivity defined as [6]

$$\Lambda_c = \frac{R^{5/6} P_c^{2/3}}{T_c^{1/6} M^{1/2} N_A^{1/3}} = 2.055\ \mathrm{mW \cdot m^{-1} \cdot K^{-1}} \tag{17}$$

The coefficients l_i in Eq. (16) are

$$l_1 = 0.0579388, \quad l_2 = -0.254517, \quad l_3 = 3.52171, \quad l_4 = -0.371906 \tag{18}$$

Equation (16) is valid in the temperature range 240 K to 410 K at densities up to $1500\ \mathrm{kg \cdot m^{-3}}$.

Figure 8 shows the selected excess data with the correlation function that is represented by a solid line. The corresponding deviation plot is

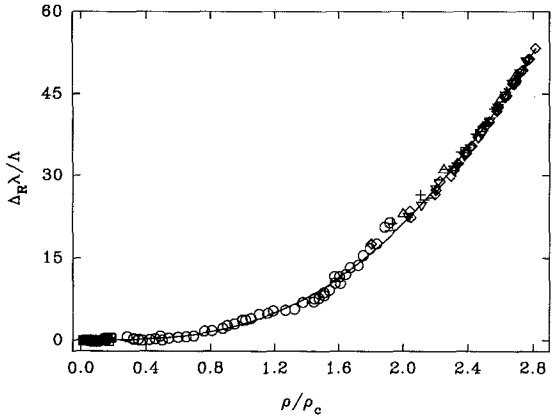

Fig. 8. The excess function for the thermal conductivity of R134a. The solid line represents values calculated from Eq. (16); the data points are those reported by Ross et al. [16], △; Taxis and Stephan [18], □; Kruppa and Straub [28], ○; Schmitt [29], ∗; Yata et al. [30], ▽; Ueno et al. [31], ◇; Oliveira et al. [32], +; and Leipertz and Kraft [33], —.

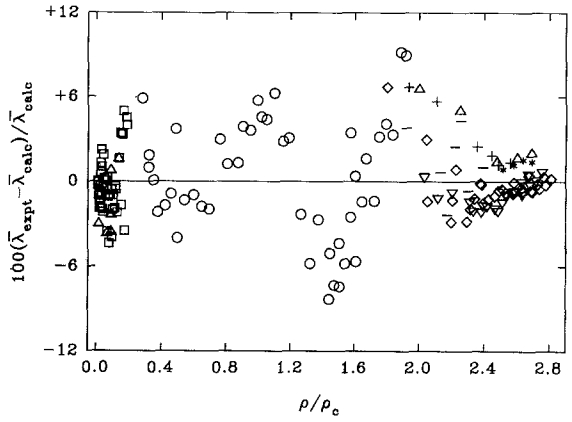

Fig. 9. Relative deviations of the experimental data of Ross et al. [16] △, Taxis and Stephan [18] □, Kruppa and Straub [28].○, Schmitt [29] ∗, Yata et al. [30] ▽, Ueno et al. [31] ◇, Oliveira et al. [32] +, and Leipertz and Kraft [33] — from values calculated with Eqs. (12) and (16) for the background thermal-conductivity $\bar{\lambda} = \eta_0 + \Delta_R\lambda$.

shown in Fig. 9. In both the vapor and the liquid phase the uncertainty is about 5%. In the critical region the uncertainty rises up to nearly 10%.

The deviations between the values of the thermal conductivity calculated from Eq. (2) and the values reported in the experimental data sets that were not used for the correlation are shown in Fig. 10. The data of Ruvinskii et al. [13], Tanaka et al. [20], and Gross et al. [17] show deviations up to 18, 10, and 9%, respectively. The saturated-liquid data of

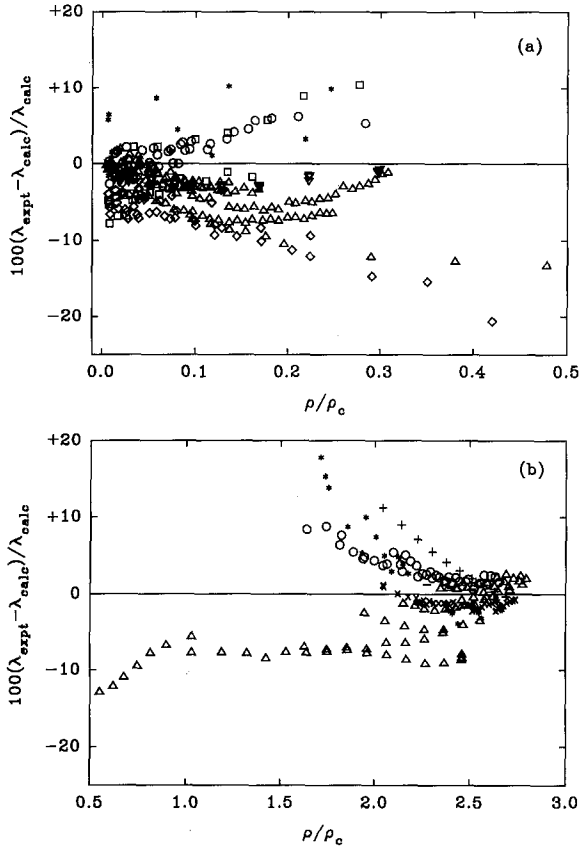

Fig. 10. Relative deviations of the experimental data of Laesecke et al. [4] △, Ruvinskii et al.. [13] *, Gross et al. [17] ○, Tanaka et al. [20] □, Yamamoto et al. [21] ◇, Heide and Lippold [34] +, Ueno et al. [35] ▽, Papadaki et al. [36] —, and Assael and Karagiannidis [37] × from values calculated with Eq. (2) for the thermal conductivity λ. (a) Results for the lower densities; (b) Results for the higher densties.

Table II. Comparison of Experimental Thermal Conductivity Data with the Correlation[a]

Ref. No.	Author	Physical state	P_{min} (MPa)	P_{max} (MPa)	T_{min} (K)	T_{max} (K)	Points compared	Method	Mean error (%)	Maximum error (%)
4	Laesecke	v, l, sv, sl	<0.1	68.4	203	393	201	hwt	4.0	−13.
13	Ruvinskii	v, l	0.1	8.9	253	400	44	hws	4.1	18.
16	Ross	v, sl	<0.1	4.6	241	373	14	hwt	2.3	6.2
17	Gross	v, l, sv, sl	0.1	6.1	253	363	83	hwt	2.6	8.8
18	Taxis	v	0.1	4.0	279	389	45	hwt	2.0	7.3
20	Tanaka	v	0.1	2.5	293	353	33	cc	4.1	10.
21	Yamamoto	v, sv	0.1	3.2	273	363	44	hwt	7.1	−20.
28	Kruppa	v, l, sv, sl	0.8	12.7	303	412	45	dls	3.6	9.0
29	Schmitt	sl	0.1	0.3	243	272	4	hwt	1.2	1.5
30	Yata	l	0.6	30.4	254	335	20	hwt	1.1	−2.2
31	Ueno	l, sl	<0.1	30	194	353	31	hwt	1.1	5.9
32	Oliveira	sl	<0.1	2.1	227	343	6	hwt	3.1	6.2
33	Leipertz	sl	0.8	3.7	303	369	9	dls	1.8	4.2
34	Heide	sl	0.1	1.7	233	333	10	cc	4.4	11.
35	Ueno	sv	0.1	2.6	253	353	34	hwt	2.2	−3.5
36	Papadaki	sl	<0.1	0.9	240	307	5	hwt	0.7	1.3
37	Assael	l, sl, v	0.1	22.4	253	333	41	hwt	1.2	−2.1

[a] v, vapor; l, liquid; sl, saturated liquid; sv, saturated vapor; cc, coaxial cylinder; hwt, hot wire (transient); hws, hot wire (steady state); dls, dynamic light scattering.

Heide and Lippold [34] show good agreement at high densities with increasing deviations in the direction of the critical point, whereas the saturated-vapor data of Yamamoto et al. [21] become up to 20% too low with increasing density. The data of Ueno et al. [35] agree fairly well with the correlation. Although they had not been used in the correlation, the data of Papadaki et al. [36] and Assael and Karagiannidis [37] are in excellent agreement with the present work. The data of Laesecke et al. [4] in the vapor phase and the 393 K isotherm run systematically lower than the values calculated from the present correlation, whereas most of their data in the liquid phase agree fairly well with it. We return to a discussion of the comparison with the data of Laesecke et al. in Section 5.2.

Just as for the viscosity, we present a compilation of the references on thermal conductivity in Table II.

5. THE CRITICAL REGION

The transport properties of fluids are influenced by long-range fluctuations in the critical region. In Section 2 we decomposed the thermal conduc-

tivity and the viscosity so that one term, namely, the critical enhancement, contains the effect of the critical fluctuations, and the other two terms, which constitute the background, are independent thereof. We now describe the critical enhancement of the transport properties using the crossover theory of Olchowy and Sengers [8, 9]. In this model the critical enhancement depends on the temperature and density through thermodynamic properties such as the specific heats and the compressibility; hence we first need to specify a fundamental equation.

5.1. Fundamental Equation

Since the critical enhancement of the thermal conductivity extends over a wide range of temperatures and densities around the critical point, we need to be able to calculate thermodynamic properties very close to the critical point as well as far away from the critical point. A fundamental equation that describes both the critical region and the classical region is not available. Instead we need to combine two equations. For temperatures and densities far away from the critical point, we use the modified BWR equation of Huber and McLinden [38], which is applicable in the vapor and liquid phases at pressures up to 70 MPa and in a temperature range from the triple point ($\approx$170 K) to 450 K. In the critical region we use a crossover equation, that is, an equation that properly describes the critical behavior of the thermodynamic properties and that has a range of validity large enough to overlap with that of a classical equation. In order to avoid large jumps in the calculated properties at the boundary where we switch between equations, we need to establish a region where both agree well and then define a switching boundary within that region. Recently, Tang et al. [24] proposed a crossover model for the thermodynamic properties of R134a in the critical region. We use that model, but we modify the system-dependent parameters in order to obtain better agreement with the classical equation of Huber and McLinden [38] in the switching region. The temperatures in the equation of Huber and McLinden are on the ITS-90 temperature scale, which gives us the opportunity to put the new crossover equation on this temperature scale by using the ITS-90 value for the critical temperature and converting the experimental temperatures using the representation given by Rusby [39].

5.1.1. Crossover Model for the Thermodynamic Properties

From the temperature T, the pressure P, the density ρ, the chemical potential μ, and the Helmholtz free energy A per unit volume V, we define the following dimensionless variables, where a subscript c indicates the value at the critical point:

$$\Delta\tilde{T} = \tilde{T} + 1 = -\frac{T_c}{T} + 1, \qquad \Delta\tilde{\rho} = \tilde{\rho} - 1 = \frac{\rho}{\rho_c} - 1$$
$$\tilde{A} = \frac{T_c A}{P_c V T}, \qquad \tilde{\mu} = \frac{\rho_c T_c \mu}{P_c T} \tag{19}$$

The dimensionless Helmholtz free-energy density and chemical potential are further decomposed as

$$\tilde{A} = \Delta\tilde{A} + \tilde{\rho}\tilde{\mu}_0(\tilde{T}) + \tilde{A}_0(\tilde{T}), \qquad \Delta\tilde{\mu} = \tilde{\mu} - \tilde{\mu}_0(\tilde{T}) \tag{20}$$

where $\tilde{A}_0(\tilde{T})$ and $\tilde{\mu}_0(\tilde{T})$ are analytic functions of the reduced temperature so that $\tilde{A}_0(-1) = -1$ and $\Delta\tilde{\mu} = 0$ at the critical temperature. We represent these background functions by truncated Taylor expansions in the reduced temperature with adjustable expansion coefficients:

$$\tilde{A}_0(\tilde{T}) = -1 + \sum_{j=1}^{4} \tilde{A}_j (\Delta\tilde{T})^j, \qquad \tilde{\mu}_0(\tilde{T}) = \sum_{j=0}^{5} \tilde{\mu}_j (\Delta\tilde{T})^j \tag{21}$$

The coefficients $\tilde{\mu}_0$ and $\tilde{\mu}_1$ are related to the zero points of energy and entropy and do not change the value of any measurable quantity. We therefore do not consider them any further. The term $\Delta\tilde{A}$ in Eq. (20) contains the effect of the critical fluctuations and is nonanalytic at the critical point. In the crossover theory of Tang et al. [24], it is represented by the following expression:

$$\Delta\tilde{A} = \frac{1}{2} t M^2 \mathscr{T}\mathscr{D} + \frac{1}{4!} u^* \bar{u} \Lambda M^4 \mathscr{D}^2 \mathscr{U} + \frac{1}{5!} a_{05} M^5 \mathscr{D}^{5/2} \mathscr{V} \mathscr{U} + \frac{1}{6!} a_{06} M^6 \mathscr{D}^3 \mathscr{U}^{3/2}$$
$$+ \frac{1}{4!} a_{14} t M^4 \mathscr{T}\mathscr{D}^2 \mathscr{U}^{1/2} + \frac{1}{2!\,2!} a_{22} t^2 M^2 \mathscr{T}^2 \mathscr{D} \mathscr{U}^{-1/2} - \frac{1}{2} t^2 \mathscr{K} \tag{22}$$

where the temperature-like variable t and the density-like variable M are related to the physical variables $\Delta\tilde{T}$ and $\Delta\tilde{\rho}$ through the following relations with system-dependent constants c_t, c_ρ, and d_1:

$$t = c_t \Delta\tilde{T}, \qquad M = c_\rho (\Delta\tilde{\rho} - d_1 \Delta\tilde{T}) \tag{23}$$

The functions $\mathscr{T}$, $\mathscr{D}$, $\mathscr{U}$, $\mathscr{V}$, and $\mathscr{K}$ can all be expressed in terms of a crossover function Y,

$$\mathscr{T} = Y^{(2-\nu^{-1})/\omega}, \qquad \mathscr{U} = Y^{1/\omega}, \qquad \mathscr{D} = Y^{-\eta/\omega}$$
$$\mathscr{V} = Y^{(\omega_a - 1/2)/\omega}, \qquad \mathscr{K} = \frac{\nu}{\alpha \bar{u} \Lambda} (Y^{-\alpha/\omega\nu} - 1) \tag{24}$$

where ν, η, α, ω, and ω_a are critical exponents and therefore universal constants, and where $\bar{u}$ is the ratio of the system-dependent coupling constant u and the universal fixed-point coupling constant u^*, $\bar{u} = u/u^*$. The crossover function Y is given implicitly by

$$1 + (\bar{u} - 1)\, Y = \bar{u} \left(1 + \frac{\Lambda^2}{\kappa^2}\right)^{1/2} Y^{1/\omega} \tag{25}$$

with

$$\kappa^2 = t\mathscr{T} + \tfrac{1}{2} u^* \bar{u} \Lambda M^2 \mathscr{D}\mathscr{U} \tag{26}$$

The other constants in Eq. (22), namely, Λ, a_{05}, a_{06}, a_{14}, and a_{22}, are system dependent.

To obtain this crossover model, Tang et al. [24] simplified the earlier proposed six-term crossover model of Chen et al. [40] by setting $c = 0$ in the so-called mixing transformation for t and M,

$$t = c_t \Delta\tilde{T} + c \left(\frac{\partial \Delta\tilde{A}}{\partial M}\right)_t, \qquad M = c_\rho (\Delta\tilde{\rho} - d_1 \Delta\tilde{T}) + c \left(\frac{\partial \Delta\tilde{A}}{\partial t}\right)_M \tag{27}$$

We can calculate all thermodynamic properties from the Helmholtz free-energy density $\tilde{A}$ in Eq. (20) using the expressions given in the Appendix of the paper by Chen et al. [40] with $c = 0$.

In our application of the model to R134a we continue to use the values adopted by Tang et al. [24] for the universal constants and the criti-

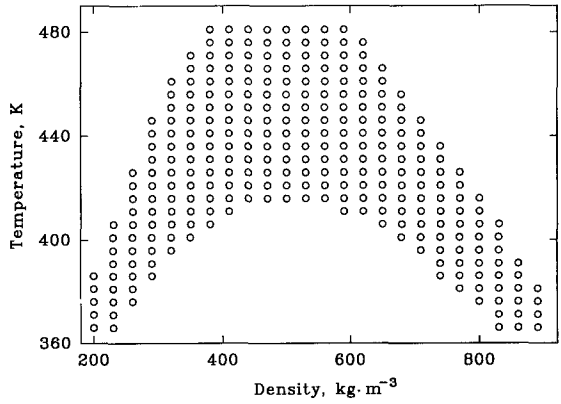

Fig. 11. Region in the temperature-density plane (○) for which values of the specific heats and the pressure were generated from the equation of Huber and McLinden [38]. The asterisk marks the critical point.

cal parameters. The adjustable parameters of the crossover model were determined from a fit to experimental data that we supplemented with values for the pressure and the specific heats generated from the equation of Huber and McLinden [38]. The region in the temperature-density plane for which values were calculated from the classical equation is shown in Fig. 11. The experimental data used in the fitting procedure are the P–ρ–T and coexistence data of Piao et al. [41], Weber [42], Basu and Wilson [43], and Tillner-Roth and Baehr [44], the vapor-pressure data of Kubota et al. [45] and Morrison and Ward [46], and the coexistence-density data of Kabata et al. [47] and Maezawa et al. [48]. The values obtained for the system-dependent coefficients are presented in Table III along with the universal constants of the crossover model. In Figs. 12–14 we present the deviations of the experimental pressure data from the values calculated with the new crossover equation for R134a. Figure 15 gives the comparison for the vapor pressure. Figure 16 shows the experimental values for the coexistence densities along with the coexistence values as calculated from our crossover model and from the classical equation of

Table III. Constants in the Thermodynamic Crossover Model for R134a

Universal critical region constants
$\nu = 0.63$, $\eta = 0.0333$, $\omega = 0.80952$, $\omega_a = 2.1$, $u^* = 0.472$
Critical parameters
$T_c = 374.274$ K, $P_c = 4.065$ MPa, $\rho_c = 515.25$ kg · m^{-3}
Crossover parameters
$\bar{u} = 0.45359$, $\Lambda = 2.3087$
Scaling-field parameters
$c_t = 2.7272$, $c_\rho = 2.2757$, $d_1 = -0.26669$
Classical parameters
$a_{05} = -1.526$, $a_{06} = 2.1498$, $a_{14} = 0.30007$, $a_{22} = 0.1768$
P–ρ–T background parameters
$\tilde{A}_1 = -6.6795$, $\tilde{A}_2 = 4.85620$, $\tilde{A}_3 = -4.6132$, $\tilde{A}_4 = 8.9002$
Caloric background parameters
$\tilde{\mu}_2 = -28.496$, $\tilde{\mu}_3 = -18.465$, $\tilde{\mu}_4 = 2.089$, $\tilde{\mu}_5 = -57.5$

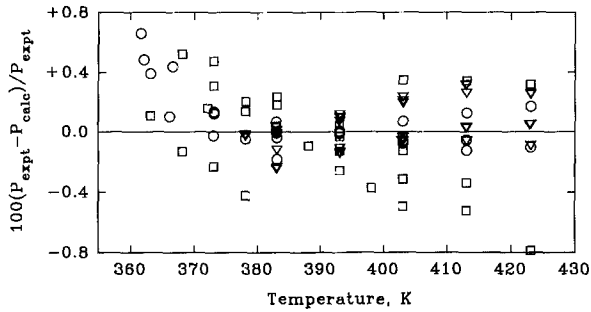

Fig. 12. Percentage deviations of the experimental pressures obtained by Piao et al. [41] (○, $\rho = 200$–$380\ \mathrm{kg \cdot m^{-3}}$; ▽, $\rho = 460$–$510\ \mathrm{kg \cdot m^{-3}}$, □, $\rho = 580$ $910\ \mathrm{kg \cdot m^{-3}}$) from the values calculated with our crossover model.

Huber and McLinden [38]. The two calculated curves differ considerably because the equations are of a different type, classical and scaling, respectively, and because Huber and McLinden used different values for the critical parameters, namely, $T_c = 374.179$ K, $\rho_c = 513.29\ \mathrm{kg \cdot m^{-3}}$, and $P_c = 4.056$ MPa, compared to our values presented in Table III.

Due to a lack of experimental data in the range of validity of the crossover model, the only caloric-property values that we used in the determination of the adjustable parameters of the model were those generated from the classical equation of Huber and McLinden [38]. Therefore a comparison with experimental caloric-property data provides a useful

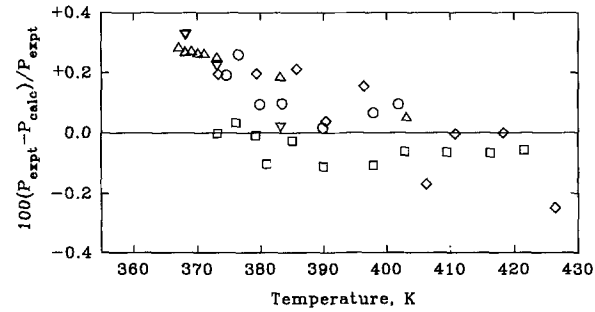

Fig. 13. Percentage deviations of the experimental pressures obtained by Weber [42] (▽, $\rho = 197\ \mathrm{kg \cdot m^{-3}}$; △, $\rho = 238\ \mathrm{kg \cdot m^{-3}}$) and by Basu and Wilson [43] (○, $\rho = 520\ \mathrm{kg \cdot m^{-3}}$; □, $\rho = 360\ \mathrm{kg \cdot m^{-3}}$; ◇, $\rho = 260\ \mathrm{kg \cdot m^{-3}}$) from the values calculated with our crossover model.

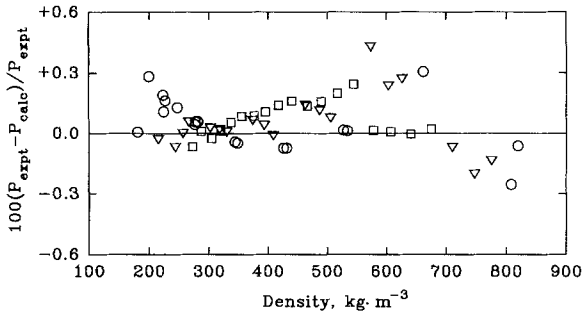

Fig. 14. Percentage deviations of the experimental pressures obtained by Tillner-Roth and Baehr [44] (○, $T = 368$–383 K; ▽, $T = 393$–413 K; □, $T = 423$–453 K) from the values calculated with our crossover model.

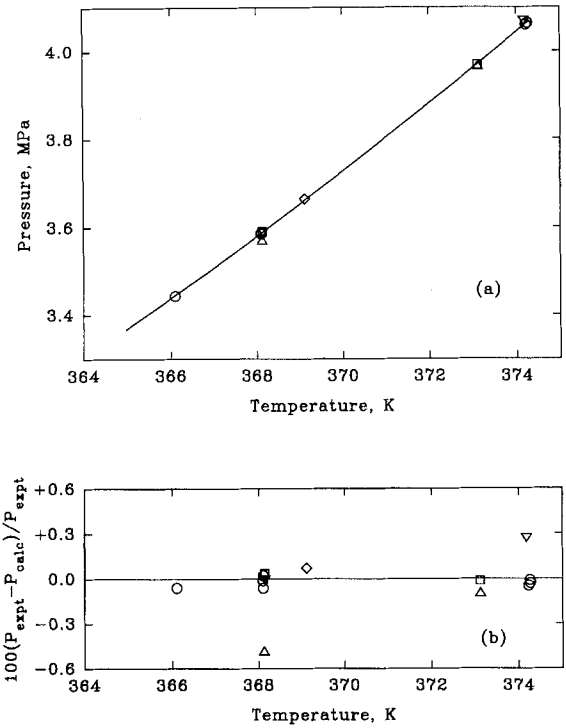

Fig. 15. (a) The vapor pressure of R134a as a function of temperature. The symbols indicate experimental data obtained by Piao et al. [41], ○; Weber [42], □; Basu et al. [43], ◇; Kubota et al. [45], △, and Morrison and Ward [46], ▽. (b) Percentage deviations of the experimental vapor pressures from the calculated values.

check of the model. In Fig. 17a we present sound-velocity data by Guedes and Zollweg [49] along with values calculated from the crossover model; in Fig. 17b, we present the corresponding deviation plot. The data on the 360 K isotherm are just outside the range of the model, as is the only experimental c_P value, obtained by Saitoh et al. [50], with which we can compare our theory. The deviation between the experimental and the calculated c_P value is -0.02%; therefore the curve of calculated values in Fig. 18 goes right through the experimental point. Based on Figs. 17 and 18, we conclude that the crossover model yields a satisfactory representation of the caloric properties of R134a in the critical region. But there remains an urgent need for additional measurements of the specific heats, especially for temperatures above 356 K.

A comparison with the original parameters of Tang et al. [24] shows that the new values are very close to the earlier ones except for the background parameters. Thus, the two versions of the crossover equation agree in the near-critical region but differ in the extended critical region where the background coefficients are important. This is due to the different data sets that were used to determine the adjustable parameters of the model. Tang et al. [24] had to determine the caloric background coefficients $\tilde{\mu}_j$ from only one isotherm of sound-velocity data [49] in the range of their

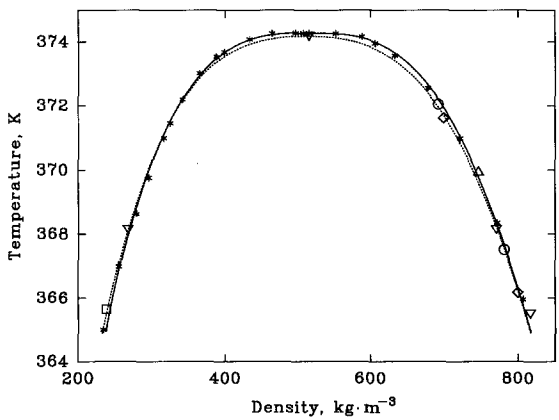

Fig. 16. The curve of coexisting vapor and liquid densities for R134a. The symbols indicate experimental values reported by Piao et al. [41], ○; Weber [42], □; Basu et al. [43], ◇; Morrison et al. [46], ▽; Kabata et al. [47], ∗; and Maezawa et al. [48], △. The solid curve represents the values for the coexistence densities as calculated from our crossover model; the dashed line represents the values from the equation of Huber and McLinden [38].

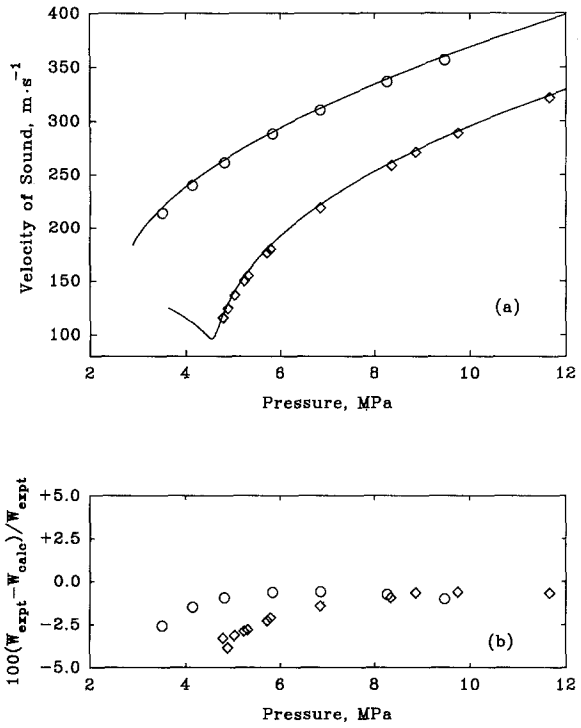

Fig. 17. (a) The velocity of sound of R134a on two isotherms as a function of pressure. The symbols indicate experimental values obtained by Guedes and Zollweg [49] (○, $T = 360.01$ K; ◇, $T = 380.17$ K). The solid curve represents the values calculated from the crossover model. (b) Percentage deviations of the experimental sound-velocity data from the calculated values.

model, whereas in this work we calculated values for the specific heats in a whole range temperatures from the equation of Huber and McLinden [38]. Consequently the agreement between the crossover equation and the data of Guedes and Zollweg is better in the version of Tang et al. [24], whereas the new version allows for a reasonable switching to the classical equation. The deviations between experimental and calculated values for the data of Piao et al. [41] and Weber [42] are also somewhat larger than for the earlier crossover equation. This is probably due to the fact that we included in the fitting procedure more experimental data than Tang et al. [24] did and included the values calculated from the equation of Huber and McLinden [38].

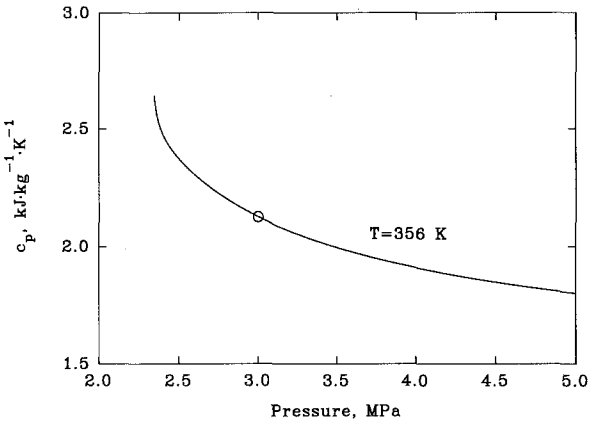

Fig. 18. The isobaric specific heat of R134a on an isotherm in the liquid phase as a function of pressure. The open circle indicates an experimental value obtained by Saitoh et al. [50]; the solid curve represents the values calculated from the crossover model.

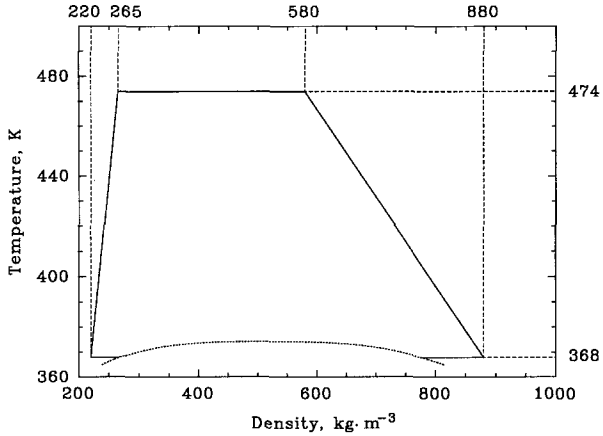

Fig. 19. Suggested boundary in the temperature-density plane for switching between the equation of Huber and McLinden [38] and the crossover model (solid lines). The coexistence curve as calculated from the crossover model (dotted line) and constant-temperature and constant-density lines (dashed lines) are included for easier orientation.

5.1.2. Switching Between the Classical and the Crossover Equation

In order to find a suitable boundary for switching between the classical equation and the crossover equation, we concentrate on two properties in particular. First, since transport properties are often measured as a function of temperature and pressure, whereas they are calculated as a function of temperature and density, a good agreement between the values of the density as calculated from temperature and pressure is essential. Second, deviations between the values for the isobaric specific heat on the boundary need to be small in order to avoid jumps in the calculated thermal-conductivity enhancement.

With this in mind, we compared values for the pressure and the isobaric specific heat as a function of temperature and density, and values for the density as a function of temperature and pressure, as calculated from each of the equations. We were able to establish a boundary with a simple geometry in the ρ–T plane (Fig. 19), where the deviations in general are within 0.2% for the pressure and density values and 1% for the isobaric specific-heat values. The exception to this is the neighborhood of the low-temperature boundary, where the proximity of the coexistence curve makes the deviations too large to be ignored. In order to connect smoothly the equations near the lower boundary, we introduce a simple switching function for densities between 220 and 880 $\mathrm{kg \cdot m^{-3}}$ and temperatures between 365 and 371 K and calculate all thermodynamic properties $x(T, \rho)$ as

$$x(T, \rho) = w(T)\, x_1(T, \rho) + (1 - w(T))\, x_2(T, \rho) \tag{28}$$

with

$$w(T) = 1 - (T - 365)/6 \tag{29}$$

where the temperature T is in K and where $x_1(T, \rho)$ and $x_2(T, \rho)$ are the values calculated from the classical and the crossover equation, respectively.

5.2. Transport Properties in the Critical Region

In the critical region we write the thermal conductivity and the viscosity as

$$\lambda = \bar{\lambda} + \Delta_c \lambda \tag{30}$$

$$\eta = \bar{\eta} + \Delta_c \eta \tag{31}$$

where $\Delta_c \lambda$ and $\Delta_c \eta$ are the critical enhancements of the thermal conductivity and the viscosity, respectively, and where $\bar{\lambda}$ and $\bar{\eta}$ are their back-

grounds. The critical enhancement $\Delta_c\lambda$ of the thermal conductivity is related to the critical part $\Delta_c D_T$ of the thermal diffusivity $D_T = \lambda/\rho c_P$ by

$$\Delta_c\lambda = \rho c_P \Delta_c D_T \tag{32}$$

where ρ is the density and c_P is the specific heat at constant pressure. Asymptotically close to the critical point the thermal diffusivity satisfies a Stokes–Einstein relation of the form [2]

$$\Delta_c D_T = \frac{R_0 kT}{6\pi\eta\xi} \tag{33}$$

where k is Boltzmann's constant, ξ is the correlation length, and where R_0 is a universal amplitude $R_0 = 1.01 \pm 0.04$ [51]. The viscosity η diverges asymptotically as

$$\eta = \Delta_c\eta + \bar{\eta} = \bar{\eta}(Q\xi)^z \tag{34}$$

where Q is a system-dependent amplitude and $z = 0.065 \pm 0.005$ is a universal critical exponent [52, 53]. In this work we adopt the values $R_0 = 1.03$ and $z = 0.063$ for these universal constants.

In the crossover theory of Olchowy and Sengers [8] the asymptotic expressions (33) and (34) are generalized to

$$\Delta_c D_T = \frac{R_0 kT}{6\pi\eta\xi}(\Omega - \Omega_0) \tag{35}$$

$$\eta = \bar{\eta}\exp(zH) \tag{36}$$

where the crossover functions $\Omega - \Omega_0$ and H depend on thermodynamic properties, on the background contributions $\bar{\lambda}$ and $\bar{\eta}$, and on a cutoff wavenumber q_D. The crossover functions are presented in their most convenient form in the Appendix of the paper by Mostert et al. [54] The correlation length ξ is calculated from the dimensionless susceptibility $\tilde{\chi}$,

$$\tilde{\chi}(T, \rho) = \frac{\rho P_c}{\rho_c^2}\left(\frac{\partial\rho}{\partial P}\right)_T \tag{37}$$

in the following way:

$$\xi = \frac{\xi_0}{\Gamma}\left(\tilde{\chi}(T, \rho) - \tilde{\chi}(T_{ref}, \rho)\frac{T_{ref}}{T}\right)^{\nu/\gamma} \tag{38}$$

where Γ and ξ_0 are system-dependent amplitudes, and ν and γ are universal critical exponents. The reference temperature T_{ref} is chosen so that for

temperatures greater than T_{ref}, the critical enhancement in the thermal conductivity is negligibly small.

The crossover model for the transport properties has been used to represent the transport properties of various fluids in the critical region [4–6, 55–57]. For R134a we determined the amplitudes from the thermodynamic crossover model with the result $\Gamma = 0.0496$, $\xi_0 = 1.94 \times 10^{-10}$ m. Based on past experience we chose $T_{ref} = (3/2)\, T_c$ for the reference temperature. The cutoff wavenumber q_D has to be determined from a comparison with experimental data.

There is only one set of experimental data for R134a in the near-critical region. Kruppa and Straub [28] used light scattering to measure the thermal diffusivity on six isotherms, on the liquid and the vapor side of the phase boundary and along the critical isotherm. From their data they deduced a critical temperature of $T_c = 374.064$ K (ITS90), which is well below the value of $T_c = 374.274$ K that we adopted. Therefore we shifted their temperatures by $+0.21$ K. Since the density values in their work are actually calculated from reduced densities, ρ/ρ_c, with the aid of a literature value of $512.2\ \mathrm{kg \cdot m^{-3}}$ for the critical density [43], we recalculated the densities using the value of $\rho_c = 515.25\ \mathrm{kg \cdot m^{-3}}$. With the aid of our fundamental equation, Section 5.1, we calculated the thermal conductivity λ from the experimental thermal diffusivity D_T through

$$\lambda = \rho c_P(T, \rho)\, D_T \tag{39}$$

The uncertainty of the values for the thermal conductivity calculated from the thermal-diffusivity data can be estimated in the following way. Kruppa and Straub [28] quote uncertainties of 0.5 to 2% for their thermal-diffusivity values, of less than 20 mK for their temperature values and of 0.3% for their density values. Since there are no experimental isobaric specific-heat data available for temperatures above 356 K, we estimate the uncertainty in the values calculated from our crossover equation through a comparison with isobaric specific-heat values calculated from the equation of Tang et al. [24] in the region where Kruppa and Straub [28] measured the thermal diffusivity. The deviations between the two equations are very small in the near-critical region, are in general smaller than 3% and rise up to 4% for data points on the 411 K isotherm and for very high and low densities. We therefore assigned a value of 3% to the uncertainty of the specific-heat values from the crossover equation. Combined with the errors in the temperature and density as quoted by Kruppa and Straub [28], the total uncertainty in the c_P values, used to convert the thermal diffusivities into thermal conductivities, varies from about 3.2% away from the critical point to about 8% on the 374.47 K isotherm. With an error of

1% for the thermal diffusivity and 0.3% for the density, the estimated uncertainties in the thermal conductivity are only slightly higher. We determined the cutoff wavenumber q_D from a comparison of the experimental data with the theoretical expression:

$$\lambda = \bar{\lambda} + \Delta_c \lambda = \lambda_0(T) + \Delta_R \lambda(\rho) + \rho c_P \Delta_c D_T \tag{40}$$

where $\lambda_0(T)$ and $\Delta_R \lambda(\rho)$ are the background functions of the thermal conductivity presented in Eqs. (12) and (16), respectively, and where $\Delta_c D_T$ is given by Eq. (35). In the fitting procedure we used data in the one-phase region with densities between 130 and 800 $kg \cdot m^{-3}$, except on the 411 K isotherm, where we excluded the data with densities higher than 520 $kg \cdot m^{-3}$. In this way we excluded the data that are likely to have higher experimental errors due to the lower intensity of the scattered light. The resulting value for the cutoff wavenumber is $q_D^{-1} = 1.9 \times 10^{-10}$ m. The constants in the crossover model for the transport properties are summarized in Table IV. In Fig. 20 we show a comparison between the thermal-conductivity values calculated from the crossover theory presented here and the thermal-conductivity data, calculated from Kruppa and Straub's [28] thermal-diffusivity data, that we used in the fitting procedure. We present a comparison between all experimental thermal-diffusivity data and the theory in Figs. 21 and 22. The agreement between theory and experimental data in the critical region is satisfactory.

The thermal-conductivity measurements reported by Laesecke et al. [4] contain data points for which a significant critical enhancement is expected. This holds in particular for their only supercritical isotherm at

Table IV. Constants in the Crossover Model for the Transport Properties of R134a

Universal constants
$R = 1.03, \quad z = 0.063, \quad \gamma = 1.239$
System-dependent amplitudes
$\Gamma = 0.0496, \quad \xi_0 = 1.94 \times 10^{-10}$ m
Reference temperature
$T_{ref} = (3/2)\, T_c$
Cutoff wavenumber
$q_D^{-1} = 1.9 \times 10^{-10}$ m

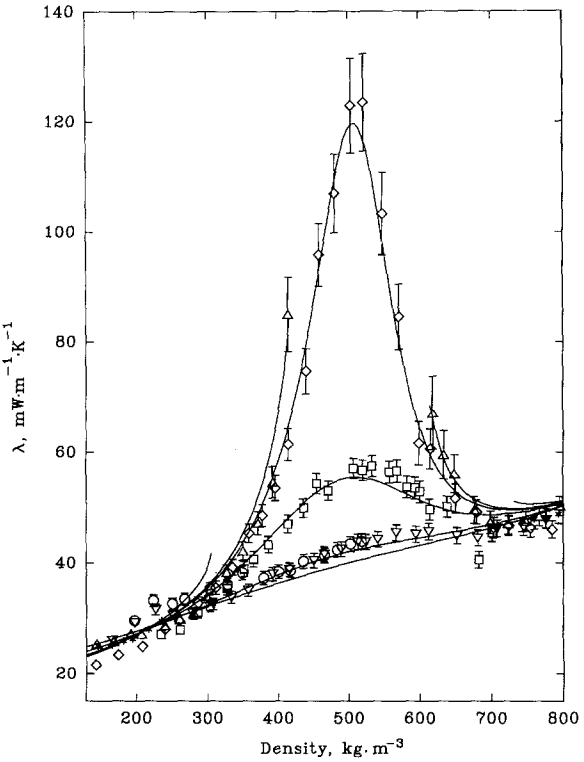

Fig. 20. The thermal conductivity of R134a in the critical region as a function of density. The symbols indicate values calculated from the experimental thermal-diffusivity data of Kruppa and Straub [28] (○, $T=412$ K; ▽, $T=393$ K; □, $T=378$ K; ◇, $T=374.65$ K; △, $T=374$ K; ∗, $T=370$ K); the solid curve represents the values calculated from the crossover model for transport properties.

393 K. Kruppa and Straub [28] obtained thermal-diffusivity data for the same isotherm that we converted to thermal-conductivity values. In Fig. 23 we present the thermal-conductivity results of Laesecke et al. [4] and of Kruppa and Straub [28] along with the values calculated from the crossover theory. As can be seen from the figure, the experimental thermal conductivities differ systematically by more than 10% for all data with densities less than $650\,\mathrm{kg\cdot m^{-3}}$. Of course, in order to make this comparison, we used calculated c_P values to convert the thermal diffusivities obtained by Kruppa and Straub into thermal conductivities. However, we believe that at most 5% of the discrepancies can be attributed to a possible

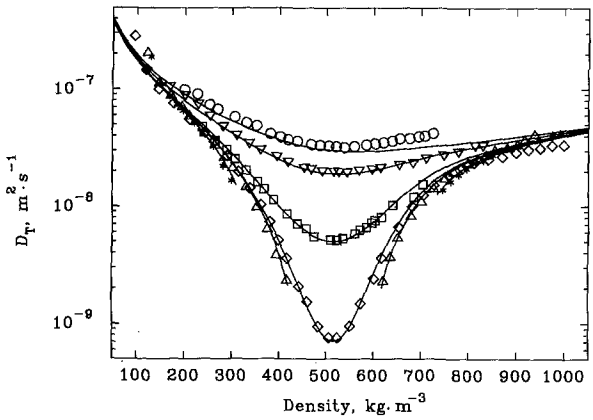

Fig. 21. The thermal diffusivity of R134a in the critical region as a function of density. The symbols indicate the experimental thermal-diffusivity data obtained by Kruppa and Straub [28] (○, $T = 412$ K; ▽, $T = 393$ K; □, $T = 378$ K; ◇, $T = 374.65$ K; △, $T = 374$ K; ∗, $T = 370$ K); the solid curve represents the values calculated from the crossover model for transport properties.

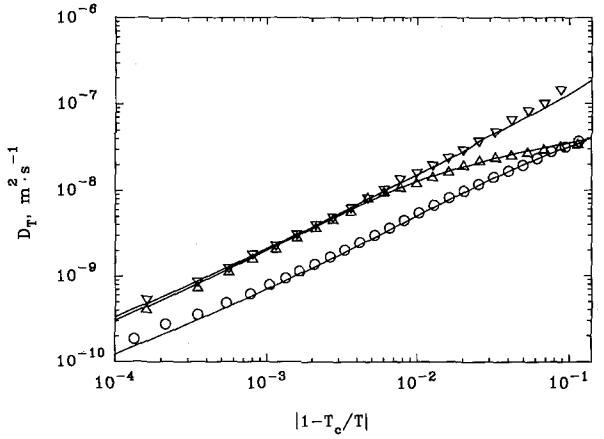

Fig. 22. The thermal diffusivity of R134a on the critical isochore and on the phase boundary as a function of the reduced temperature. The symbols indicate the experimental values obtained by Kruppa and Straub [28] (○, critical isochore; △, liquid phase; ▽, vapor phase); the solid curves represent the values calculated from the crossover model for transport properties.

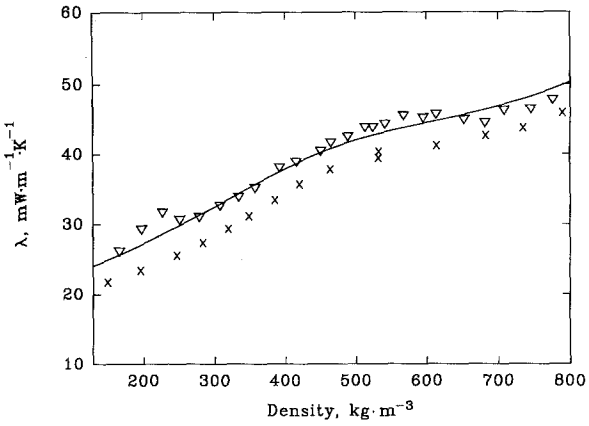

Fig. 23. The thermal conductivity of R134a on the $T = 393$ K isotherm as a function of density. (∇) values calculated from the experimental thermal-diffusivity data of Kruppa and Straub [28]; ($\times$) experimental data of Laesecke et al. [4]. The solid curve represents the values calculated from the crossover model for transport properties.

uncertainty in c_P, and we are unable to reconcile the two data sets on the basis of the currently available information. We conclude that additional measurements of the thermal conductivity in this region are desirable.

6. RESULTS

The viscosity η of R134a can be calculated from Eq. (1), where the correlation for the dilute-gas function $\eta_0(T)$ is presented by Eqs. (7)–(11) and the correlation for the excess function $\Delta_R\eta(\rho)$ is presented by Eqs. (13)–(15). An estimate for the critical enhancement $\Delta_c\eta$ can be obtained from the crossover theory for transport properties Eq. (36). The correlation for the viscosity is valid for temperatures from 290 K to 430 K and for densities up to 1400 kg·m^{-3}. The thermal conductivity λ is given by Eq. (2), where the correlation for the dilute-gas function $\lambda_0(T)$ is presented by Eq. (12), the correlation for the excess function $\Delta_R\lambda(\rho)$ is presented by Eqs. (16)–(18), and the critical enhancement $\Delta_c\lambda$ can be calculated from Eq. (32). The correlation for the thermal conductivity is valid for temperatures from 240 to 410 K and for densities up to 1500 kg·m^{-3}.

We present tables of values for the viscosity and the thermal conductivity calculated from Eqs. (1) and (2), respectively, in Tables V–VII. Table V contains the saturation properties as a function of temperature,

Table V. Saturation Properties of R134a

T (K)	P (MPa)	ρ' (kg·m^{-3})	ρ'' (kg·m^{-3})	η' (μPa·s)	η'' (μPa·s)	λ' (mW·m^{-1}·K^{-1})	λ'' (mW·m^{-1}·K^{-1})
240	0.0724752	1395.	3.837			108.1	8.866
242	0.0798549	1389.	4.203			107.3	9.041
244	0.0878133	1383.	4.596			106.4	9.216
246	0.0964010	1378.	5.018			105.5	9.390
248	0.105641	1372.	5.470			104.7	9.642
250	0.115568	1366.	5.953			103.8	9.824
252	0.126216	1360.	6.470			102.9	10.01
254	0.137623	1354.	7.021			102.1	10.19
256	0.149823	1348.	7.609			101.2	10.37
258	0.162856	1342.	8.235			100.3	10.55
260	0.176759	1335.	8.902			99.43	10.74
262	0.191571	1329.	9.610			98.56	10.92
264	0.207332	1323.	10.36			97.69	11.10
266	0.224083	1317.	11.16			96.81	11.29
268	0.241864	1310.	12.01			95.93	11.48
270	0.260718	1304.	12.90			95.06	11.66
272	0.280687	1297.	13.85			94.18	11.85
274	0.301815	1291.	14.85			93.30	12.04
276	0.324144	1284.	15.91			92.41	12.23
278	0.347720	1278.	17.03			91.53	12.42
280	0.372588	1271.	18.22			90.65	12.61
282	0.398794	1264.	19.46			89.76	12.81
284	0.426384	1257.	20.78			88.87	13.00
286	0.455368	1250.	22.17			87.98	13.20
288	0.485879	1243.	23.63			87.09	13.40
290	0.517915	1236.	25.17	216.8	11.77	86.20	13.60
292	0.551524	1229.	26.79	211.6	11.86	85.30	13.81
294	0.586756	1222.	28.49	206.5	11.95	84.40	14.02
296	0.623662	1214.	30.29	201.6	12.04	83.50	14.23
298	0.662293	1207.	32.17	196.7	12.14	82.60	14.44
300	0.702702	1199.	34.16	191.9	12.23	81.70	14.66
302	0.744940	1192.	36.24	187.2	12.33	80.79	14.88
304	0.789066	1184.	38.44	182.7	12.43	79.88	15.10
306	0.835118	1176.	40.75	178.1	12.52	78.97	15.33
308	0.883166	1168.	43.17	173.7	12.63	78.05	15.57
310	0.933261	1160.	45.73	169.4	12.73	77.14	15.80
312	0.985456	1151.	48.41	165.1	12.83	76.22	16.05
314	1.03981	1143.	51.23	160.9	12.94	75.29	16.30
316	1.09637	1134.	54.20	156.8	13.05	74.37	16.56
318	1.15520	1125.	57.33	152.8	13.16	73.44	16.82
320	1.21643	1117.	60.62	148.8	13.28	72.51	17.09
322	1.28003	1107.	64.09	144.9	13.40	71.58	17.38
324	1.34608	1098.	67.74	141.0	13.52	70.65	17.67
326	1.41462	1088.	71.59	137.2	13.65	69.72	17.97

Table V. *(Continued)*

T (K)	P (MPa)	ρ' (kg·m^{-3})	ρ'' (kg·m^{-3})	η' (μPa·s)	η'' (μPa·s)	λ' (mW·m^{-1}·K^{-1})	λ'' (mW·m^{-1}·K^{-1})
328	1.48581	1079.	75.66	133.5	13.78	68.78	18.28
330	1.55965	1069.	79.95	129.8	13.92	67.84	18.60
332	1.63622	1058.	84.50	126.2	14.07	66.90	18.94
334	1.71558	1048.	89.30	122.6	14.22	65.97	19.30
336	1.79782	1037.	94.40	119.0	14.38	65.03	19.67
338	1.88301	1026.	99.81	115.5	14.55	64.09	20.06
340	1.97124	1014.	105.6	112.0	14.73	63.16	20.47
342	2.06250	1003.	111.7	108.6	14.92	62.22	20.91
344	2.15707	990.3	118.2	105.2	15.12	61.30	21.37
346	2.25492	977.6	125.2	101.8	15.35	60.37	21.87
348	2.35615	964.3	132.7	98.38	15.58	59.46	22.40
350	2.46086	950.5	140.8	95.01	15.84	58.55	22.98
352	2.56916	936.0	149.6	91.64	16.13	57.66	23.61
354	2.68116	920.8	159.0	88.26	16.45	56.78	24.30
356	2.79699	904.7	169.4	84.85	16.80	55.91	25.08
358	2.91678	887.6	180.8	81.41	17.20	55.05	25.94
360	3.04066	869.2	193.5	77.92	17.65	54.21	26.94
362	3.16880	849.2	207.8	74.33	18.18	53.39	28.10
364	3.30138	827.3	224.0	70.62	18.81	52.60	29.51
366	3.43842	802.8	243.4	66.75	19.60	51.86	32.53
368	3.58016	775.0	266.8	62.66	20.61	51.24	36.22
370	3.72746	742.0	295.7	58.20	21.96	50.98	40.28
372	3.88128	697.9	336.2	52.82	24.07	51.98	47.45
374	4.04227	604.9	425.9	43.85	30.13	75.02	95.31

where a single prime and a double prime indicate values on the liquid and on the vapor side of the coexistence curve, respectively. The critical enhancement of the viscosity as estimated from our crossover model is included in the values; its contribution to the total viscosity exceeds 1% on the coexistence curve for temperatures above 372 K, and on the critical isochore for temperatures below 379 K. In Tables VI and VII we give the values for the viscosity and the thermal conductivity, respectively, as a function of temperature and pressure. Please note that for any data in the vapor phase at atmospheric pressures or below only the dilute-gas functions are used. Because of inconsistencies in the data sets used, the overall uncertainties of the present correlations cannot be better than approximately $\pm 5\%$ for the background terms.

Table VI. Viscosity of R134a (μPa·s)

	T(K)																				
P(MPa)	290	298	300	305	310	315	320	325	330	335	340	350	360	370	380	390	400	410	420	430
0.1	11.65	11.98	12.06	12.25	12.45	12.65	12.84	13.04	13.23	13.43	13.62	14.00	14.38	14.75	15.12	15.49	15.85	16.21	16.57	16.93
0.5	11.76	12.08	12.15	12.35	12.54	12.74	12.93	13.12	13.32	13.51	13.70	14.07	14.45	14.82	15.19	15.55	15.91	16.27	16.63	16.98
1.0	218.6	197.6	193.1	181.1	169.7	12.95	13.13	13.31	13.49	13.68	13.86	14.22	14.59	14.95	15.31	15.67	16.02	16.37	16.72	17.07
1.5	220.5	199.6	195.0	183.1	171.7	160.7	150.1	139.7	13.86	14.01	14.17	14.49	14.82	15.16	15.50	15.85	16.19	16.53	16.87	17.21
2.0	222.4	201.5	197.0	185.1	173.7	162.8	152.2	142.0	132.0	122.1	112.2	14.97	15.22	15.50	15.80	16.12	16.43	16.75	17.08	17.40
2.5	224.3	203.4	198.9	187.0	175.7	164.8	154.4	144.2	134.3	124.6	115.0	95.30	15.91	16.04	16.25	16.50	16.78	17.06	17.36	17.66
3.0	226.1	205.3	200.7	188.9	177.7	166.8	156.4	146.4	136.6	127.1	117.7	98.79	17.43	16.97	16.95	17.07	17.25	17.48	17.73	17.99
3.5	228.0	207.1	202.6	190.8	179.6	168.8	158.4	148.5	138.8	129.4	120.2	101.9	82.55	19.05	18.10	17.90	17.92	18.03	18.21	18.41
4.0	229.8	208.9	204.4	192.7	181.5	170.7	160.4	150.5	140.9	131.7	122.6	104.8	86.67	64.57	20.44	19.21	18.86	18.78	18.83	18.95
4.5	231.6	210.8	206.3	194.5	183.3	172.6	162.4	152.5	143.0	133.8	124.9	107.5	90.22	71.24	31.48	21.56	20.26	19.80	19.64	19.63
5.0	233.4	212.6	208.1	196.3	185.2	174.5	164.3	154.5	145.1	135.9	127.1	110.1	93.39	76.03	54.50	26.63	22.48	21.23	20.69	20.47
5.5	235.2	214.3	209.9	198.1	187.0	176.3	166.2	156.4	147.0	138.0	129.3	112.5	96.29	79.92	62.02	38.33	26.13	23.26	22.10	21.53
6.0	236.9	216.1	211.6	199.9	188.8	178.2	168.0	158.3	149.0	140.0	131.3	114.8	98.99	83.36	67.16	48.83	32.08	26.14	23.94	22.88
6.5	238.7	217.9	213.4	201.7	190.6	180.0	169.8	160.2	150.9	142.0	133.4	117.0	101.5	86.45	71.28	55.51	39.50	30.10	26.32	24.55
7.0	240.4	219.6	215.1	203.4	192.3	181.7	171.6	162.0	152.7	143.9	135.3	119.2	103.9	89.28	74.85	60.46	46.10	34.96	29.30	26.58
7.5	242.2	221.3	216.9	205.2	194.1	183.5	173.4	163.8	154.6	145.7	137.3	121.2	106.2	91.90	78.05	64.49	51.40	40.03	32.81	28.98
8.0	243.9	223.1	218.6	206.9	195.8	185.2	175.2	165.6	156.4	147.6	139.1	123.2	108.4	94.36	80.94	67.96	55.74	44.73	36.60	31.71
8.5	245.6	224.8	220.3	208.6	197.5	186.9	176.9	167.3	158.1	149.4	141.0	125.2	110.5	96.70	83.62	71.12	59.44	48.89	40.39	34.66
9.0	247.4	226.5	222.0	210.3	199.2	188.6	178.6	169.0	159.9	151.2	142.8	127.1	112.5	98.92	86.11	73.99	62.69	52.54	44.00	37.69
9.5	249.1	228.2	223.7	212.0	200.9	190.3	180.3	170.7	161.6	152.9	144.6	128.9	114.5	101.0	88.46	76.64	65.62	55.80	47.33	40.70
10.0	250.8	229.8	225.3	213.6	202.5	192.0	182.0	172.4	163.3	154.6	146.3	130.7	116.4	103.1	90.70	79.12	68.37	58.75	50.40	43.59
11.0	254.1	233.2	228.7	216.9	205.8	195.3	185.3	175.7	166.6	158.0	149.7	134.3	120.1	107.0	94.87	83.65	73.31	63.95	55.83	48.94
12.0	257.5	236.5	232.0	220.2	209.1	198.5	188.5	179.0	169.9	161.3	153.0	137.6	123.6	110.6	98.73	87.76	77.70	68.58	60.52	53.69
13.0	260.8	239.7	235.2	223.4	212.3	201.7	191.7	182.2	173.1	164.5	156.3	140.9	126.9	114.1	102.4	91.57	81.70	72.75	64.79	57.89
14.0	264.1	243.0	238.4	226.6	215.5	204.9	194.8	185.3	176.2	167.6	159.4	144.1	130.2	117.4	105.8	95.14	85.40	76.58	68.69	61.78
15.0	267.4	246.2	241.6	229.8	218.6	208.0	197.9	188.4	179.3	170.7	162.5	147.2	133.3	120.6	109.1	98.51	88.87	80.14	72.31	65.39
16.0	270.6	249.3	244.8	232.9	221.7	211.1	201.0	191.4	182.3	173.7	165.5	150.2	136.4	123.7	112.2	101.7	92.16	83.48	75.69	68.77
17.0	273.9	252.5	247.9	236.0	224.8	214.1	204.0	194.4	185.3	176.7	168.5	153.2	139.3	126.7	115.3	104.8	95.28	86.65	78.88	71.95
18.0	277.1	255.6	251.1	239.1	227.8	217.1	207.0	197.4	188.3	179.6	171.4	156.1	142.2	129.7	118.2	107.8	98.28	89.68	81.91	74.97
19.0	280.3	258.8	254.2	242.2	230.8	220.1	210.0	200.3	191.2	182.5	174.3	159.0	145.1	132.5	121.0	110.6	101.2	92.57	84.82	77.86
20.0	283.5	261.9	257.2	245.2	233.8	223.1	212.9	203.2	194.1	185.4	177.1	161.8	147.9	135.3	123.8	113.4	104.0	95.37	87.60	80.62
22.0	289.8	268.0	263.3	251.2	239.8	228.9	218.7	208.9	199.7	191.0	182.6	167.2	153.3	140.7	129.2	118.8	109.3	100.7	92.89	85.86
24.0	296.1	274.1	269.4	257.2	245.6	234.7	224.3	214.5	205.3	196.4	188.1	172.6	158.6	145.9	134.3	123.9	114.4	105.7	97.88	90.79
26.0	302.4	280.2	275.4	263.1	251.4	240.4	230.0	220.1	210.7	201.8	193.4	177.8	163.7	150.9	139.3	128.8	119.2	110.5	102.6	95.46
28.0	308.6	286.2	281.4	268.9	257.1	246.0	235.5	225.5	216.1	207.1	198.7	182.9	168.7	155.8	144.1	133.5	123.9	115.1	107.2	99.93
30.0	314.8	292.1	287.3	274.7	262.8	251.6	241.0	230.9	221.4	212.4	203.8	187.9	173.6	160.6	148.8	138.2	128.4	119.6	111.5	104.2

Table VII. Thermal Conductivity of R134a ($mW \cdot m^{-1} \cdot K^{-1}$)

	T(K)																			
P(MPa)	240	250	260	270	273	280	290	298	300	310	320	330	340	350	360	370	380	390	400	410
0.1	108.1	9.736	10.59	11.43	11.69	12.25	13.06	13.71	13.86	14.63	15.40	16.14	16.88	17.59	18.30	18.98	19.65	20.31	20.95	21.58
0.5	108.3	104.0	99.61	95.20	93.80	90.73	13.57	14.16	14.30	15.02	15.73	16.43	17.13	17.81	18.48	19.14	19.79	20.42	21.05	21.66
1.0	108.5	104.2	99.87	95.49	94.10	91.06	86.56	82.81	81.95	77.20	16.54	17.13	17.73	18.34	18.95	19.55	20.14	20.73	21.31	21.89
1.5	108.7	104.5	100.1	95.78	94.40	91.39	86.92	83.22	82.37	77.69	72.84	18.38	18.74	19.18	19.67	20.18	20.70	21.22	21.74	22.25
2.0	108.9	104.7	100.4	96.07	94.70	91.71	87.29	83.62	82.78	78.17	73.40	68.44	63.20	20.54	20.75	21.07	21.46	21.88	22.31	22.75
2.5	109.2	104.9	100.7	96.36	95.00	92.02	87.64	84.02	83.19	78.63	73.94	69.09	64.00	58.63	22.47	22.36	22.49	22.74	23.05	23.39
3.0	109.4	105.2	100.9	96.64	95.29	92.34	87.99	84.40	83.58	79.08	74.47	69.71	64.76	59.57	26.31	24.40	23.94	23.88	23.99	24.19
3.5	109.6	105.4	101.2	96.92	95.57	92.65	88.34	84.78	83.97	79.53	74.98	70.31	65.48	60.46	55.23	28.97	26.14	25.41	25.18	25.16
4.0	109.7	105.6	101.4	97.19	95.86	92.95	88.68	85.16	84.35	79.96	75.48	70.89	66.17	61.29	56.26	51.00	30.24	27.59	26.71	26.35
4.5	109.9	105.8	101.7	97.46	96.14	93.25	89.01	85.52	84.73	80.38	75.97	71.45	66.83	62.07	57.20	52.18	48.45	30.99	28.74	27.82
5.0	110.1	106.1	101.9	97.74	96.42	93.55	89.34	85.89	85.10	80.80	76.44	72.00	67.46	62.82	58.09	53.29	48.34	37.14	31.51	29.78
5.5	110.3	106.3	102.1	98.00	96.69	93.85	89.67	86.24	85.46	81.21	76.90	72.53	68.07	63.54	58.93	54.31	49.61	43.94	35.20	31.93
6.0	110.5	106.5	102.4	98.27	96.97	94.14	89.99	86.59	85.82	81.61	77.35	73.04	68.67	64.22	59.73	55.24	50.75	46.08	39.44	34.53
6.5	110.8	106.7	102.6	98.53	97.24	94.43	90.31	86.94	86.17	82.00	77.80	73.54	69.24	64.88	60.49	56.11	51.77	47.52	42.57	37.35
7.0	111.0	106.9	102.9	98.79	97.51	94.71	90.62	87.28	86.52	82.39	78.23	74.03	69.79	65.51	61.21	56.94	52.76	48.68	44.51	39.93
7.5	111.2	107.2	103.1	99.05	97.77	94.99	90.93	87.61	86.86	82.77	78.65	74.51	70.33	66.12	61.91	57.52	53.65	49.69	45.92	41.96
8.0	111.4	107.4	103.3	99.30	98.03	95.27	91.24	87.95	87.20	83.14	79.07	74.97	70.85	66.72	62.58	58.48	54.48	50.61	47.05	43.52
8.5	111.6	107.6	103.6	99.56	98.29	95.55	91.54	88.27	87.53	83.51	79.48	75.43	71.36	67.29	63.22	59.20	55.28	51.54	48.02	44.76
9.0	111.8	107.8	103.8	99.81	98.55	95.82	91.84	88.59	87.86	83.87	79.88	75.87	71.86	67.84	63.84	59.89	56.04	52.37	48.90	45.79
9.5	112.0	108.0	104.0	100.1	98.80	96.09	92.13	88.91	88.18	84.23	80.27	76.31	72.34	68.38	64.45	60.56	56.77	53.15	49.72	46.70
10.0	112.2	108.2	104.3	100.3	99.06	96.36	92.43	89.23	88.50	84.58	80.66	76.73	72.82	68.91	65.03	61.20	57.47	53.91	50.58	47.52
11.0	112.6	108.6	104.7	100.8	99.56	96.89	93.00	89.84	89.13	85.26	81.41	77.56	73.73	69.92	66.15	62.43	58.81	55.34	52.08	49.09
12.0	113.0	109.0	105.1	101.3	100.0	97.40	93.56	90.45	89.74	85.93	82.14	78.36	74.61	70.88	67.20	63.58	60.06	56.67	53.47	50.53
13.0	113.4	109.3	105.6	101.7	100.5	97.91	94.12	91.04	90.34	86.58	82.85	79.14	75.45	71.81	68.21	64.67	61.23	57.92	54.79	51.87
14.0	113.8	109.7	106.0	102.2	101.0	98.41	94.66	91.61	90.92	87.22	83.54	79.88	76.27	72.69	69.17	65.71	62.35	59.11	56.03	53.15
15.0	114.2	110.2	106.4	102.7	101.5	98.90	95.19	92.18	91.50	87.84	84.21	80.61	77.05	73.54	70.09	66.70	63.41	60.23	57.20	54.36
16.0	114.6	110.6	106.8	103.1	101.9	99.39	95.71	92.73	92.06	88.44	84.86	81.32	77.81	74.36	70.97	67.65	64.42	61.30	58.32	55.51
17.0	114.9	111.0	107.2	103.5	102.4	99.86	96.22	93.27	92.61	89.03	85.50	82.00	78.55	75.16	71.82	68.56	65.39	62.33	59.39	56.62
18.0	115.3	111.4	107.6	104.0	102.8	100.3	96.72	93.80	93.15	89.61	86.12	82.67	79.27	75.92	72.64	69.44	66.32	63.30	60.42	57.67
19.0	115.7	111.8	108.0	104.4	103.3	100.8	97.21	94.33	93.67	90.18	86.73	83.32	79.96	76.67	73.44	70.28	67.21	64.25	61.40	58.69
20.0	116.0	112.1	108.3	104.8	103.7	101.2	97.70	94.84	94.19	90.73	87.32	83.95	80.64	77.39	74.21	71.10	68.08	65.15	62.34	59.67
22.0	116.8	112.9	109.1	105.6	104.5	102.1	98.65	95.84	95.21	91.81	88.47	85.18	81.95	78.78	75.68	72.66	69.72	66.87	64.14	61.52
24.0	117.5	113.7	109.9	106.4	105.3	103.0	99.56	96.81	96.18	92.86	89.58	86.36	83.20	80.10	77.07	74.12	71.26	68.48	65.81	63.25
26.0	118.2	114.4	110.7	107.2	106.1	103.8	100.5	97.74	97.13	93.86	90.64	87.49	84.39	81.36	78.40	75.52	72.72	70.01	67.39	64.88
28.0	118.8	115.1	111.5	107.9	106.9	104.6	101.3	98.65	98.05	94.83	91.67	88.57	85.54	82.57	79.67	76.84	74.10	71.45	68.88	66.42
30.0	119.5	115.8	112.2	108.7	107.6	105.4	102.2	99.53	98.94	95.78	92.67	89.62	86.64	83.73	80.88	78.11	75.42	72.82	70.30	67.88

7. CONCLUSION

Based on a critical review of the available experimental data, and on as much theory as realistically possible, equations for the viscosity and the thermal conductivity of R134a were developed. The existing, somewhat contradictory situation of the transport properties of R134a could be clarified only to some extent. We need more precise measurements of both the viscosity and the thermal conductivity in nearly the entire fluid region. Measurements of the specific heats for temperatures above 356 K are also urgently needed.

In the case of the viscosity, systematic deviations between the experimental results of different authors are evident in the entire density range of the correlation (Fig. 7) and even at ambient pressure (Fig. 2). Measurements are also needed to fill the data gap in the vapor phase (Figs. 6 and 7). For the thermal conductivity in the dilute-gas region the biggest inconsistencies exist at the lower and upper ends of the range of validity of Eq. (12) (Fig. 4). For the excess thermal conductivity systematic deviations between different data sets are evident in the entire density range (Fig. 10). Experimental data are lacking in particular in the critical and supercritical region. It is very promising that the Subcommittee on Transport Properties of the Commision I.2 of the International Union of Pure and Applied Chemistry has recently started a project to investigate the phenomena in detail that occur in the measurements of the thermal conductivity of refrigerants in the vapor phase. This will certainly contribute to clarify the above-mentioned situation.

ACKNOWLEDGMENTS

We are indebted to B. Kruppa and J. Straub for providing us with light-scattering data prior to publication, to M. L. Huber for the computer program for the classical equation, and to R. A. Perkins for some valuable comments. The research at the University of Maryland was supported by the Division of Chemical Sciences of the Office of Basic Energy Sciences of the U.S. Department of Energy under Grant DE-FG05-88ER13902. The research at the University of Stuttgart was supported by the German-Israeli Foundation (GIF Contract No. I-124-042.10/89).

The work has been carried out under the auspices of the Subcommittee on Transport Properties of Commission I.2 of the International Union of Pure and Applied Chemistry.

REFERENCES

1. K. Stephan and R. Krauss, *Proc. Symp. Solid Sorption Refrig.* (International Institute of Refrigeration, Comm. B1, Paris, 1992), p. 32 [also to be published as a special issue of *J. Heat. Recov. Syst.* (1993)].
2. J. V. Sengers, *Int. J. Thermophys.* **6**:203 (1985).
3. C. A. Nieto de Castro, in *Supercritical Fluid Technology*, T. J. Bruno and J. F. Ely, eds. (CRC Press, Boca Raton FL, 1991), p. 335.
4. A. Laesecke, R. A. Perkins, and C. A. Nieto de Castro, *Fluid Phase Equil.* **80**:263 (1992).
5. V. Vesovic, W. A. Wakeham, G. A. Olchowy, J. V. Sengers, J. T. R. Watson, and J. Millat, *J. Phys. Chem. Ref. Data* **19**:763 (1990).
6. A. Laesecke, R. Krauss, K. Stephan, and W. Wagner, *J. Phys. Chem. Ref. Data* **19**:1089 (1990).
7. J. O. Hirschfelder, C. F. Curtiss, and R. B. Bird, *Molecular Theory of Gases and Liquids* (Wiley, New York, 1954).
8. G. A. Olchowy and J. V. Sengers, *Phys. Rev. Lett.* **61**:15 (1988).
9. G. A. Olchowy and J. V. Sengers, *Int. J. Thermophys.* **10**:417 (1989).
10. H. Nabizadeh and F. Mayinger, *High Temp. High Press.* **24**:221 (1992).
11. M. Takahashi, C. Yokoyama, and S. Takahashi, *Proc. High Press. Conf. (30)* (Sendai, Japan, 1989), p. 372.
12. D. C. Dowdell and G. P. Matthews, *J. Phys. Chem. Ref. Data* (to be published).
13. G. Ya. Ruvinskii, G. K. Lavrenchenko, and S. V. Iljushenko, *Kholod. Tekh.* 20 (1990); translated in G. K. Lavrenchenko, G. Ya. Ruvinskii, S. V. Iljushenko' and V. V. Kanaev, *Int. J. Refrig.* **15**:1 (1992).
14. C. M. B. P. Oliveira and W. A. Wakeham, *Int. J. Thermophys.* **14**:33 (1993).
15. E. Bich, J. Millat, and E. Vogel, *Wiss. Z. Wilh.-Pieck-Univ. Rostock* **36**:5 (1987).
16. M. Ross, J. P. M. Trusler, W. A. Wakeham, and M. Zalaf, *Proc. Meet. Int. Inst. Refrig. Comm. B1 Tel-Aviv* **1**:89 (1990).
17. U. Gross, Y. W. Song, and E. Hahne, *Int. J. Thermophys.* **13**:957 (1992).
18. B. Taxis and K. Stephan, *Int. J. Refrig.* (to be published).
19. I. R. Shankland, R. S. Basu, and D. P. Wilson, *Proc. Meet. Int. Inst. Refrig. Comm. B1, B2, E1, E2, Purdue* **2**:305 (1988).
20. Y. Tanaka, M. Nakata, and T. Makita, *Int. J. Thermophys.* **12**:949 (1991).
21. R. Yamamoto, S. Matsuo, and Y. Tanaka, *Int. J. Thermophys.* **14**:79 (1993).
22. C. M. B. P. Oliveira and W. A. Wakeham, *Int. J. Thermophys.* **14**:33 (1993).
23. T. Okubo, T. Hasuo, and A. Nagashima, *Int. J. Thermophys.* **13**:931 (1992).
24. S. Tang, G. J. Jin, and J. V. Sengers, *Int. J. Thermophys.* **12**:515 (1991).
25. A. Kumagai and S. Takahashi, *Int. J. Thermophys.* **12**:105 (1991).
26. D. E. Diller, A. S. Aragon, and A. Laesecke, *Fluid Phase Equil.* (in press).
27. D. Ripple, *Rev. Sci. Instrum.* **63**:3153 (1992); D. Ripple and O. Matar, *J. Chem. Eng. Data* (in press).
28. B. Kruppa and J. Straub, *Fluid Phase Equil.* **80**:305 (1992).
29. M. Schmitt, *Diplomarbeit* (Inst. Techn. Thermodyn. Therm. Verfahrenst., University of Stuttgart, 1990).
30. J. Yata, Ch. Kawashima, M. Hori, and T. Minamiyama, *Proc. Asian Thermophys. Prop. Conf. (2)* (1989), p. 201.
31. Y. Ueno, M. Sekikawa, Y. Nagasaka, and A. Nagashima, *Proc. Jap. Symp. Thermophys. Prop. (11)* (1990), p. 123.
32. C. M. B. P. Oliveira, M. Papadaki, and W. A. Wakeham, *Proc. Asian Thermophys. Prop. Conf.* (3) (1992), p. 32.
33. A. Leipertz and K. Kraft, private communication (1992).

34. R. Heide and H. Lippold, *Proc. Meet. Int. Inst. Refrig. Comm. B2, E2, D1, D2/3, Dresden* **4**:237 (1990).
35. Y. Ueno, Y. Nagasaka, and A. Nagashima, *Proc. Jap. Symp. Thermophys. Prop. (12)* (1991), p. 225.
36. M. Papadaki, M. Schmitt, A. Seitz, K. Stephan, B. Taxis, and W. A. Wakeham, *Int. J. Thermophys.* **14**:173 (1993).
37. M. J. Assael and E. Karagiannidis, *Int. J. Thermophys.* **14**:183 (1993).
38. M. L. Huber and M. O. McLinden, *Proc. 1992 International Refrigeration Conference. Purdue University, U.S.A., July 14–17, 1992*, Vol. II, p. 453.
39. R. L. Rusby, *J. Chem. Thermodyn.* **23**:1153 (1991).
40. Z. Y. Chen, A. Abbaci, S. Tang, and J. V. Sengers, *Phys. Rev. A* **42**:4470 (1990).
41. C.-C. Piao, H. Sato, and K. Watanabe, *ASHRAE Trans.* **96** (Part 1):132 (1990).
42. L. A. Weber, *Int. J. Thermophys.* **10**:617 (1989).
43. R. S. Basu and D. P. Wilson, *Int. J. Thermophys.* **10**:591 (1989).
44. R. Tillner-Roth and H. D. Baehr, *J. Chem. Thermodyn.* **24**:413 (1992).
45. H. Kubota, T. Yamashita, Y. Tanaka, and T. Makita, *Int. J. Thermophys.* **10**:629 (1989).
46. G. Morrison and D. K. Ward, *Fluid Phase Equil.* **62**:65 (1991).
47. Y. Kabata, S. Tanikawa, M. Uematsu, and K. Watanabe, *Int. J. Thermophys.* **10**:605 (1989).
48. Y. Maezawa, H. Sato, and K. Watanabe, *J. Chem. Eng. Data* **35**:225 (1990).
49. H. J. R. Guedes and J. A. Zollweg, *Int. J. Refrig.* **15**:381 (1992).
50. A. Saitoh, S. Nakagawa, H. Sato, and K. Watanabe, *J. Chem. Eng. Data* **35**:107 (1990).
51. H. C. Burstyn, J. V. Sengers, J. K. Bhattacharjee, and R. A. Ferrell, *Phys. Rev. A* **28**:1567 (1983).
52. R. F. Berg and M. R. Moldover, *Phys. Rev. A* **42**:7183 (1990).
53. J. C. Nieuwoudt and J. V. Sengers, *J. Chem. Phys.* **90**:457 (1989).
54. R. Mostert, H. R. van den Berg, P. S. van der Gulik, and J. V. Sengers, *J. Chem. Phys.* **92**:5454 (1990).
55. J. Luettmer-Strathmann and J. V. Sengers, *Proceedings, Workshop on the Thermophysical Properties of Environmentally Acceptable Refrigerants, Ericeira, Portugal, 1992* (submitted).
56. R. A. Perkins, D. G. Friend, H. M. Roder, and C. A. Nieto de Castro, *Int. J. Thermophys.* **12**:965 (1991).
57. R. A. Perkins, H. M. Roder, and D. G. Friend, *Physica A* **173**:332 (1991).